Summary Results Report STS-79/Mir 4 and STS-89/Mir8 Missions

Mechanics of Granular Materials (MGM)

NAS8-38779

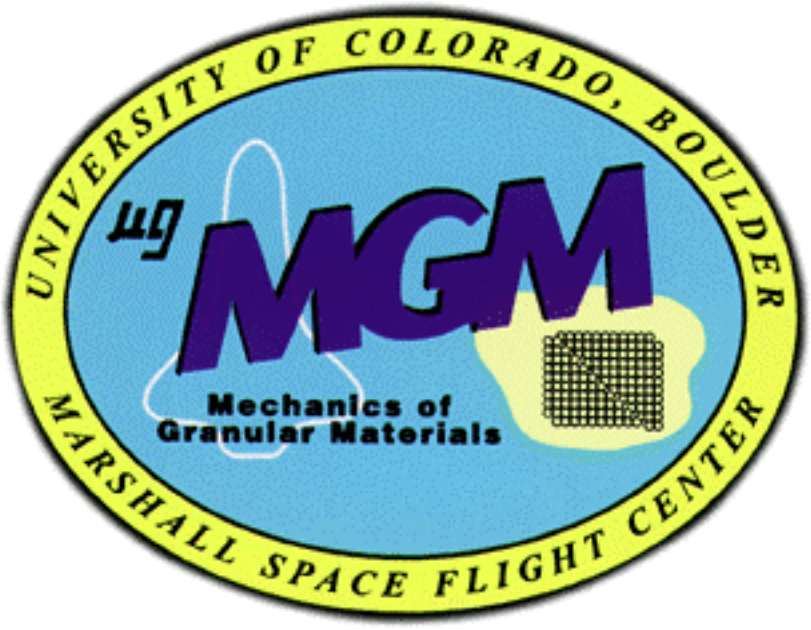

Principal Investigator:	Stein Sture University of Colorado at Boulder
Co-Investigator:	Nicholas C. Costes George C. Marshall Space Flight Center
Project Scientist:	Khalid A. Alshibli University of Alabama at Huntsville
Co-Authors:	Susan N. Batiste Melissa Frank Mark R. Lankton Roy A. Swanson

1 Introduction

1.1 Overview

Unlike materials such as metals, polymers, cementitious concrete, rocks, etc., the strength and deformation characteristics of which are derived mainly from strong cohesive forces from chemical cementation, the constitutive behavior of uncemented granular materials, including strength, stiffness modulus behavior, dilatancy, localization of deformation, shear band formation, and instability behavior are to a large extent derived from interparticle friction resulting from normal forces acting on particles or particle groups. Particle bonding by short or long-term Coulombic forces and van der Waal-type forces may also play a role to a certain extent; however, the main sources of the constitutive relations and stability properties of cohesionless granular materials is interparticle friction, which, in turn, under low confining effective stress levels is highly dependent on gravitational body forces. Erosional processes and off-road locomotion are illustrative examples.

1.2 Hypothesis

The force-displacement behavior of granular materials is fabric or structure dependent, highly nonlinear, dilatant and non-conservative. The gravity-induced stresses in laboratory specimens are nearly of the same order of magnitude as the externally applied tractions, thus limiting the size of the specimens. On the other hand, the same laboratory specimens must be sufficiently large to replicate the behavior of large geologic deposits *in situ* or the behavior of large masses of industrial or agricultural products during storage, handling and transportation.

During critical, unstable states such as liquefaction of saturated loose sands under earthquakes and wave loading, landslides due to pore water pressure build-up, or the collapse of sensitive clays, gravity acts as a follower load, thus making the sequence of such phenomena impossible to observe and study as they occur either in the laboratory or in the field.

In granular materials, gravity-driven particle convection induces material inhomogeneities and anisotropies during experiments, especially under very low confining pressures, which alter the initial fabric of the specimens and hence their constitutive relations. Accordingly, from an engineering point of view, uncertainties of unknown magnitude are introduced regarding the actual behavior of the large masses in the field the specific experiments are intended to emulate.

Under moderate-to-high stress levels, the influence of gravity on the behavior of experiments may not be pronounced and, therefore, the test results in a terrestrial (1 g) environment may be sufficiently conclusive for engineering purposes. However, testing of granular materials under very low stress levels can only be performed in a microgravity environment. It should be emphasized again that the laboratory specimen that on one hand would resemble a magnified version of the elemental cube in a mechanics sense, should on the other hand, be representative of the real mass particle fabric. The gravity induced stresses within the specimen transform the experiment into a complex boundary value problem, where the constitutive properties and stability issues cannot be resolved by inverse identification techniques due to the highly nonlinear nature of the constitutive and stability behavior. For the same reasons, one cannot determine the constitutive relations of granular

materials at very low effective stress levels by extrapolating results from centrifuge experiments performed at high stress levels.

The same arguments could be made for the influence of gravitational body forces on a multitude of issues associated with granular materials under very low effective stress levels. Such issues include: determination of critical porosity or void ratio in granular materials and their relation to the maximum porosity of the same materials, both with and in the absence of shear-band formation; bifurcation instability and associated shear-band formation and strain softening at persistent and controlled effective stress states.

1.3 Objects of Investigation

A series of displacement-controlled triaxial compression experiments were performed in the SPACEHAB module of the Orbiter, during STS-79 and STS-89 missions to Mir. The experiments were conducted on nine right cylindrical specimens 75 mm in diameter and 150 mm long at confining pressures ranging from 0.189 psi to 0.007 psi (1.30 kPa to 0.05 kPa) at relative densities of 85% (STS-79) and 65% (STS-89). The displacement-controlled test configuration was chosen in order to maintain overall specimen-apparatus stability as well as local material stability in the event continuous or discontinuous bifurcation instability were to take place associated with respectively diffuse bulging or localization of deformation in narrow shear bands, which might lead to overall strain-softening and brittleness phenomena. In these tests the displacements are controlled through stiff and highly polished tungsten carbide end-platens, while a constant confining pressure is transmitted through a flexible, relatively thin, latex rubber membrane surrounding the cylindrical surface between the ends. In the three STS-79 and first three of six STS-89 experiments (denoted "F1" and "F2", respectively) five axial compression, loading and unloading cycles were completed at regular intervals up to an overall compressive strain of 25%. In the last three of six STS-89 experiments (denoted "F3"), ten 0.5 mm loading and unloading cycles were followed by seven 5 mm loading and unloading cycles. Detailed recording of data especially related to volume change were obtained during the loading, unloading and reloading cycles to study how complex and often counter-intuitive dilatancy phenomena originate. Specifically, the volume change (dilatancy) loops achieved in such loading cycles tend to magnify at low stress levels, which make it possible to observe them and possibly arrive at unambiguous conclusions regarding the kinematic-static mechanisms controlling deformation and strength behavior, especially at the low effective stress states associated with fluidization and liquefaction phenomena. In this manner, the specimens comprise a mixed, but well defined boundary value problem. The specimens consist of subrounded quartz sand, which were tested in the dry condition. During testing axial load, axial displacement, confining pressure, bulk volumetric changes, 360 degree video coverage, ambient pressure, temperature and acceleration levels were recorded.

Optical techniques monitored overall behavior of the specimens, specifically to track any onset of formation of shear bands. A regular grid was printed on the membrane surface, which facilitated tracking of motion throughout the specimens' surfaces. After the experiments were completed, the specimens were subjected to non-destructive x-ray tomography and epoxy-impregnated. Later they will be cut into thin sections for further internal examination of pore space distribution, internal fabric features and zones of instability.

1.4 Background/History of Project

The MGM experiment was initiated by Dr. Nicholas C. Costes in 1976. The PI, Stein Sture joined Dr. Costes' effort in 1977. It was reviewed and adopted by NASA's Physics and Chemistry Experiments in Space (PACE) working group in 1977. The MGM project has in the intervening years been subjected to 7 science peer reviews, including a high level review effort conducted by Dr. Robert Schrieffer (Nobel Prize, 1974). Eighteen different academicians and four industry researchers have participated at the various peer reviews. In addition, the project has been subjected to numerous internal NASA (MSFC, ARC, NASA Headquarters) and NAS/NRC program reviews. While the project started at MSFC, it was for two years (1980-1982) managed by ARC, but returned to MSFC. The project was selected for space flight in 1991, when detailed apparatus concept design efforts began. While all early science efforts took place at MSFC and the University of Colorado at Boulder, apparatus design and manufacturing was carried out at Sandia National Laboratories. The Laboratory for Atmospheric and Space Physics (LASP) of the University of Colorado at Boulder became an important partner in the project in 1993, aiding in the first set of MGM experiments on STS-79, where three tests were successfully carried out. LASP assumed responsibility for missions following STS-79, successfully carrying out six additional experiments on STS-89.

2 Methods/Research Operations, STS-79

2.1 List & Description of All Functional Objectives

2.1.1 FO1 – Perform flight 1 experiment

Experiments are performed by compressing the sand specimen axially. This functional objective is achieved when the mechanical equipment, flight software, and test cell function together and compress the specimens. This functional objective is primary, as FO #2,3,4,6,7,8,9,10 can not be achieved without basic experiment performance.

2.1.2 FO2 – Run three tests, identical aside from confining pressure

Plans include testing all three test specimens aboard the flight. In order to have comparable results, all tests need to be performed on identical specimens following the same procedure each time. However, because the effect of confining pressures on specimen performance is of great interest, the confining pressures are to be different for each test (0.007 psi, 0.075 psi, 0.189 psi).

2.1.3 FO3 – Record data on memory cards

Data monitoring specimen behavior and equipment performance are recorded onto memory cards. In order to maximize science return, load cell and pressure transducer voltage, compression motor position, and water jacket accumulator position during each test must be recorded. The load cell measures the axial force transmitted to the specimen. Pressure transducers monitor pressure within the water jacket and specimen, recording the effective confining force on the specimen. The compression motor position measures the displacement, or compression, inflicted on the specimen. The water jacket accumulator may be used to record the volume change of the specimen during testing. By recording load, pressure, displacement and volume data, information such as peak and residual strengths, shear band, stress-strain moduli (Young's Modulus, Poissons Ratio, Shear Modulus), and dilatancy will be calculated. This information will then be used to model granular material under low confining pressures.

2.1.4 FO4 – Record video data

During testing, cameras record video of the specimen compression. Each specimen is contained in a latex membrane with a grid pattern printed upon it, in order to facilitate analysis. This data is used to assist in corrections applied to data recorded on the memory cards, such as confining pressure, as the latex membrane adds slight confinement to the specimen as axial compression proceeds and the specimen expands. Also, the video data is used to track deformation patterns.

2.1.5 FO5 – Record SAMS data

SAMS is located directly above the TDLA containing the MGM experiment. During an experiment, the specimen is put into an unstable condition, and small accelerations may disturb the specimen. By recording SAMS data, a check can be performed to evaluate whether data collected is a result of testing procedure or an outside occurrence, including accelerations. This knowledge is also important, during post-flight examination of the specimen.

2.1.6 FO6 – Retrieve deformed specimens post-flight

Science data are collected not only by collecting data during testing, but also by examining the specimen after the experiment is complete. This will only be possible if the specimens are retrieved.

2.1.7 FO7 – Measure surface contour of deformed specimens post-flight

Before stabilization, surface measurements are taken. This provides information to complement video data, and supplement post-stabilization data, as a small outer layer of the specimen is lost during stabilization.

2.1.8 FO8 – Stabilize deformed specimens post-flight

Stabilizing the deformed specimens permanently fixes the granular particles in the post-test configuration, which will allow further examination of the specimens in their compressed form.

2.1.9 FO9 – Perform x-ray Computed Tomography scans on stabilized specimens post-flight

CT scanning is a non-destructive examination technique which allows a first look inside the specimens by providing internal density information on a low resolution basis. This information is used to find trends within the specimens, such as patterns of lower or higher density material that may indicate a shear band. These trends will also be used to plan cuts on specimens for maximum data retrieval during the (destructive) internal examination portion of analysis.

2.1.10 FO10 – Perform (destructive) internal examination of stabilized specimens post-flight

Very precise information on the internal formations in the stabilized specimens will be collected during this phase of examination. The specimen will be cut into, and examined under a microscope. Data including void ratio and particle alignment, shear band location and width will be collected during this phase of testing.

2.2 List & Description of all Hardware Items Used

2.2.1 HW1 – MGM Twin Double Locker Assembly (TDLA)

PI-Provided.
Built by Sandia National Laboratories, Albuquerque, NM

The TDLA consists of two open-fronted box structures each occupying the space of two Middeck Locker Equivalents (MLEs). These structures are designated Locker 1 and Locker 2. They are mounted side by side with approximately 1 inch separation. For the MGM-I mission on STS-79 the TDLA was mounted on the forward bulkhead of the SPACEHAB module. Locker 1 contains the Combined Electronics Unit (CEU), the water jacket and specimen accumulators and plumbing, the pressure sensors, and the Power Interface Panel (PIP). Locker 2 contains the test cell, viewing stage, experiment clock display, and the 3 built-in video cameras which view the test cell during each experiment. During the compression phase of the experiments the open front of Locker 2 is covered by a beta cloth light cover. The TDLA also provides launch/landing mounting points for 3 test cells, 1 test cell in Locker 1 and 2 test cells in Locker 2.

The TDLA PIP has a single 28V input power connector. It also provides a serial interface connector for the Payload and General Support Computer (PGSC), and a video output connector and cable which connects to the Video Interface Unit (VIU).

2.2.2 HW2 – MGM Test Cell ID#0

PI-provided.
Built by Sandia National Laboratories, Albuquerque, NM
Specimen preparation and final assembly performed at the Laboratory for Atmospheric and Space Physics, University of Colorado, Boulder, CO

The MGM Test Cell contains the cylindrical granular material specimen. The specimen is contained within a surrounding latex membrane and two end platens, one fixed and one movable. The structure of the test cell consists of a transparent Lexan water jacket with aluminum top and bottom end plates. This structure surrounds the specimen and is filled with water to provide controlled confining pressure on the specimen. The structure also supports a motor-driven mechanism which drives the movable end platen to compress the specimen axially during the experiment.

The cylindrical granular material specimen consists of dry Ottawa F-75 Sand. The specimen is 75 mm in diameter and 150 mm in height at the start of the experiment. The water surrounding the specimen is pressurized to 15 psig to stabilize the specimen during storage, launch and landing. During an experiment, this pressure is reduced to the level specified for the experiment: .007 psid (differential pressure) for Experiment 1, .075 psid for Experiment 2, and .189 for Experiment 3.

Five test cells were prepared for the MGM-I mission. Three test cells were selected for the flight, with the remaining 2 test cells reserved as flight spares.

Test Cell ID#0 was used for the .007 psid flight experiment on the MGM-I mission.

2.2.3 HW3 – MGM Test Cell ID#4

PI-provided.
Built by Sandia National Laboratories, Albuquerque, NM
Specimen preparation and final assembly performed at the Laboratory for Atmospheric and Space Physics, University of Colorado, Boulder, CO

See 2.2.2 for test cell description.

Test Cell ID#4 was used for the .075 psid flight experiment on the MGM-I mission.

2.2.4 HW4 – MGM Test Cell ID#7

PI-provided.
Built by Sandia National Laboratories, Albuquerque, NM
Specimen preparation and final assembly performed at the Laboratory for Atmospheric and Space Physics, University of Colorado, Boulder, CO

See 2.2.2 for test cell description.

Test Cell ID#7 was used for the .189 psid flight experiment on the MGM-I mission.

2.2.5 HW5 – MGM Accumulator Purge Fittings

PI-provided.
Built by Sandia National Laboratories, Albuquerque, NM

The accumulator purge fittings are used in the deactivation phase of each experiment as part of the procedure to restore the accumulators to their default starting configuration. There are 2 purge fittings, 1 for the water

jacket accumulator and 1 for the specimen accumulator. The purge fittings are stowed in the MGM stowage box, separate from the TDLA and test cells.

2.2.6 HW6 – Drink Bag

PI-provided.

The accumulator purge procedure, which is performed during the deactivation phase of each experiment, expels excess water from the water jacket accumulator. A standard crew drink bag is connected to the purge fitting attached to the water jacket accumulator to collect this water. One drink bag is used for each of the 3 experiments. The drink bags are stowed in the MGM stowage box, separate from the TDLA and test cells.

2.2.7 HW7 – Memory Card

PI-provided.
Intel commercial off-the-shelf item.

For each flight experiment, 2 memory cards are installed in the CEU in Locker 1. The memory cards are redundant; an identical complete set of experiment data is stored on each card. The memory cards provide non-volatile storage for the recorded flight data. A total of 6 memory cards are used. Each card has a capacity of 10 megabytes. The memory cards are stored in a custom-designed holder in Locker 1 and are returned to the holder after use.

2.2.8 HW8 – Canon L-1 Camcorder

STS-provided.
Canon commercial off-the-shelf item.

For each experiment, the MGM video output is recorded on Hi-8 video tape using an STS-provided camcorder in VCR mode. The MGM video output consists of the signals from the 3 built-in video cameras in Locker 2, multiplexed into a single output signal. The MGM video output and the camcorder are connected via the VIU.

2.2.9 HW9 – Hi-8 Video Tape Cassette

STS-provided.
Commercial off-the-shelf item.

For each experiment, the MGM video output is recorded on one 120-minute Hi-8 video tape cassette.

2.2.10 HW10 – Payload and General Support Computer (PGSC)

STS-provided.
IBM commercial off-the-shelf item.

The PGSC is used by the Mission Specialist to control each MGM experiment. The software program is run from a floppy disk. The PGSC is connected to the PIP mounted on Locker 1 by a serial interface cable.

2.2.11 HW11 – MGM PGSC Floppy Disks

PI-provided.
Commercial off-the-shelf item containing PI-provided software.

The MGM PGSC Floppy Disk contains the UI2 software program used by the Mission Specialist to control the experiments. Two identical disks are provided.

2.2.12 HW12 – PGSC Serial Cable

STS-provided.

The PGSC serial cable is used to connect the PGSC to the serial port on the PIP.

2.2.13 HW13 – MGM PIP-VIU Video Cable

PI-provided.

The MGM PIP-VIU Video Cable is used to connect the VIU to the video output port on the PIP.

2.2.14 HW14 – MGM Bench Test System

PI-provided.
Built by Sandia National Laboratories, Albuquerque, NM

The MGM Bench Test System is used for 1-g ground testing of specimens and as a testbed for experimental techniques and software. The Bench Test System consists of flight-like CEU, accumulators, sensors and plumbing. The plumbing on the Bench Test System is configured horizontally to minimize the effects of water head on confining pressure in the 1-g tests.

2.2.15 HW15 – MGM Test Cell ID#2

PI-provided.
Built by Sandia National Laboratories, Albuquerque, NM
Specimen preparation and final assembly performed at the Laboratory for Atmospheric and Space Physics, University of Colorado, Boulder, CO

See 2.2.2 for test cell description.

Test Cell ID#2 was reserved as a flight spare and used in the ground truth test following the flight.

2.2.16 HW16 – MGM Test Cell ID#3

PI-provided.
Built by Sandia National Laboratories, Albuquerque, NM
Specimen preparation and final assembly performed at the Laboratory for Atmospheric and Space Physics, University of Colorado, Boulder, CO

See 2.2.2 for test cell description.

Test Cell ID#3 was reserved as a flight spare and stabilized in its original, undeformed state following the flight.

2.2.17 HW17 – Space Acceleration Measurement System (SAMS)

NASA-provided.

The SAMS equipment provides a record of the acceleration environment in which the MGM experiments are performed. The data recorded by this equipment is retrieved electronically from Lewis Research Center (LeRC) after the flight, and is used in the MGM data analysis.

2.3 Sessions/Functional Objectives (FO) Table

Mission	Session Name	FO#	HW#	Scheduled day	Actual day	Samples/Parameters	Method
STS-79	Specimen Preparation	2	HW2, HW3, HW4, HW15, HW16	L - 45 start	6/15/96 - 7/10/96		Specimen Prep. (2.4.1)
STS-79	Experiment 1	1, 2, 3, 4	HW1, HW2, HW5-HW13	FD 2 9/18/96	FD 2 9/18/96	Confining pressure 0.007 psid	Quasi-static axial compression (2.4.2)
STS-79	Experiment 2	1, 2, 3, 4	HW1, HW3, HW5-HW13	FD 4 9/20/96	FD 4 9/20/96	Confining pressure 0.075 psid	Quasi-static axial compression (2.4.2)
STS-79	Experiment 3	1, 2, 3, 4	HW1, HW4, HW5-HW13	FD 5 9/21/96	FD 5 9/21/96	Confining pressure 0.189 psid	Quasi-static axial compression (2.4.2)
STS-79	Experiments 1,2,3	5	HW17	FD2, FD4, FD5	FD2, FD4, FD5	SAMS head 3, 25 Hz bandwidth	SAMS data acquisition (2.4.3)
STS-79	Specimen 3 stabilization	6, 7, 8, 9, 10	HW4	R + 4 weeks	10/25/96		Epoxy impregnation (2.4.5)
STS-79	Specimen 2 stabilization	6, 7, 8, 9, 10	HW3	R + 6 weeks	11/1/96		Epoxy impregnation (2.4.5)
STS-79	Specimen 1 stabilization	6, 7, 8, 9, 10	HW2	R + 8 weeks	11/11/96		Epoxy impregnation (2.4.5)
STS-79	Ground truth test	2,3	HW14, HW15	R + 8 weeks	11/18/96	Confining pressure 0.189 psid, 1-g test	Quasi-static axial compression (2.4.4)
STS-79	Flight spare specimen stabilization	6, 7, 8, 9, 10	HW16	R + 10 weeks	11/26/96		Epoxy impregnation (2.4.5)
STS-79	Ground truth specimen stabilization	6, 7, 8, 9, 10	HW15	R + 12 weeks	12/24/96		Epoxy impregnation (2.4.5)

Table 1. Sessions/Functional Objectives (FO), MGM-I, STS-79.

3 Methods/Research Operations, STS-89

3.1 List & Description of All Functional Objectives

3.1.1 FO1 – Perform flight experiment

Experiments are performed by compressing the sand specimen axially. This functional objective is achieved when the mechanical equipment, flight software, and test cell function together and compress the specimens. This functional objective is primary, as FO #2,3,4,5,7,8,9,10 can not be achieved without basic experiment performance.

3.1.2 FO2 – Run three F2 tests, identical aside from confining pressure

Plans include testing all three test specimens aboard the flight. In order to have comparable results, all tests need to be performed on identical specimens following the same procedure each time. However, because the effect of confining pressures on specimen performance is of great interest, the confining pressures are to be different for each test (0.007 psi, 0.075 psi, 0.189 psi).

3.1.3 FO3 – Run three F3 tests, identical aside from confining pressure

Plans include testing all three test specimens aboard the flight. In order to have comparable results, all tests need to be performed on identical specimens following the same procedure each time. However, because the effect of confining pressures on specimen performance is of great interest, the confining pressures are to be different for each test (0.007 psi, 0.075 psi, 0.189 psi).

3.1.4 FO4 – Record data on memory cards

Data monitoring specimen behavior and equipment performance are recorded onto memory cards. In order to maximize science return, load cell and pressure transducer voltage, compression motor position, and water jacket accumulator position during each test must be recorded. The load cell measures the axial force transmitted to the specimen. Pressure transducers monitor pressure within the water jacket and specimen, recording the effective confining force on the specimen. The compression motor position measures the displacement, or compression, inflicted on the specimen. The water jacket accumulator may be used to record the volume change of the specimen during testing. By recording load, pressure, displacement and volume data, information such as peak and residual strengths, shear band, stress-strain moduli (Young's Modulus, Poisson's Ratio, Shear Modulus), and dilatancy will be calculated. This information will then be used to model granular material under low confining pressures.

3.1.5 FO5 – Record video data

During testing, cameras record video of the specimen compression. Each specimen is contained in a latex membrane with a grid pattern printed upon it, in order to facilitate analysis. This data is used to assist in corrections applied to data recorded on the memory cards, such as confining pressure, as the latex membrane adds slight confinement to the specimen as axial compression proceeds and the specimen expands. Also, the video data is used to track deformation patterns.

3.1.6 FO6 – Record SAMS data

SAMS is located directly below the TDLA containing the MGM experiment. During an experiment, the specimen is put into an unstable condition, and small accelerations may disturb the specimen. By recording SAMS data, a check can be performed to evaluate whether data collected is a result of

testing procedure or an outside occurrence, including accelerations. This knowledge is also important, during post-flight examination of the specimen.

3.1.7 FO7 – Retrieve deformed specimens post-flight

Science data are collected not only by collecting data during testing, but also by examining the specimen after the experiment is complete. This will only be possible if the specimens are retrieved.

3.1.8 FO8 – Perform x-ray Computed Tomography scans on stabilized specimens post-flight

CT scanning is a non-destructive examination technique which allows a first look inside the specimens by providing internal density information on a low resolution basis. This information is used to find trends within the specimens, such as patterns of lower or higher density material that may indicate a shear band. These trends will also be used to plan cuts on specimens for maximum data retrieval during the (destructive) internal examination portion of analysis.

3.1.9 FO9 – Stabilize deformed specimens post-flight

Stabilizing the deformed specimens permanently fixes the granular particles in the post-test configuration, which will allow further examination of the specimens in their compressed form.

3.1.10 FO10 – Perform (destructive) internal examination of stabilized specimens post-flight

Very precise information on the internal formations in the stabilized specimens will be collected during this phase of examination. The specimen will be cut into, and examined under a microscope. Data including void ratio and particle alignment, shear band location and width will be collected during this phase of testing.

3.2 List & Description of all Hardware Items Used

3.2.1 HW1 – MGM Twin Double Locker Assembly (TDLA)

PI-Provided.
Built by Sandia National Laboratories, Albuquerque, NM

The TDLA consists of two open-fronted box structures each occupying the space of two Middeck Locker Equivalents (MLEs). These structures are designated Locker 1 and Locker 2. They are mounted side by side with approximately 1 inch separation. For the MGM-II mission on STS-89 the TDLA was mounted on the aft bulkhead of the SPACEHAB module. Locker 1 contains the Combined Electronics Unit (CEU), the water jacket and specimen accumulators and plumbing, the pressure sensors, and the Power Interface Panel (PIP). Locker 2 contains the test cell, viewing stage, experiment clock display, and the 3 built-in video cameras which view the test cell during each experiment. During the compression phase of the experiments the open front of Locker 2 is covered by a beta cloth light cover. The TDLA also provides launch/landing mounting points for 3 test cells, 1 test cell in Locker 1 and 2 test cells in Locker 2.

The TDLA PIP has a single 28V input power connector. It also provides a serial interface connector for the Payload and General Support Computer (PGSC), and a video output connector and cable which connects to the Video Interface Unit (VIU).

3.2.2 HW2 – MGM Test Cell ID#0

PI-provided.
Built by Sandia National Laboratories, Albuquerque, NM and the Laboratory for Atmospheric and Space Physics, University of Colorado, Boulder, CO
Specimen preparation and final assembly performed at the Laboratory for Atmospheric and Space Physics, University of Colorado, Boulder, CO

The MGM Test Cell contains the cylindrical granular material specimen. The specimen is contained within a surrounding latex membrane and two end platens, one fixed and one movable. The structure of the test cell consists of a transparent Lexan water jacket with aluminum top and bottom end plates. This structure surrounds the specimen and is filled with water to provide controlled confining pressure on the specimen. The structure also supports a motor-driven mechanism which drives the movable end platen to compress the specimen axially during the experiment.

The cylindrical granular material specimen consists of dry Ottawa F-75 Sand. The specimen is 75 mm in diameter and 150 mm in height at the start of the experiment. The water surrounding the specimen is pressurized to 15 psig to stabilize the specimen during storage, launch and landing. During an experiment, this pressure is reduced to the level specified for the experiment: .007 psid (differential pressure) for Experiment 1, .075 psid for Experiment 2, and .189 for Experiment 3.

Eight test cells were prepared for the MGM-II mission. Six test cells were selected for the flight (three for the F2 and three for the F3 experiments), with the remaining two test cells reserved as flight spares. The F3 test cells were stored in the TDLA (HW1) and the F2 test cells were stored in foam-padded lockers.

Test Cell ID#0 was used for the .007 psid F2 flight experiment on the MGM-II mission.

3.2.3 HW3 – MGM Test Cell ID#1

PI-provided.
Built by Sandia National Laboratories, Albuquerque, NM and the Laboratory for Atmospheric and Space Physics, University of Colorado, Boulder, CO
Specimen preparation and final assembly performed at the Laboratory for Atmospheric and Space Physics, University of Colorado, Boulder, CO

See 2.2.2 for test cell description.

Test Cell ID#1 was used for the .075 psid F2 flight experiment on the MGM-II mission.

3.2.4 HW4 – MGM Test Cell ID#2

PI-provided.
Built by Sandia National Laboratories, Albuquerque, NM and the Laboratory for Atmospheric and Space Physics, University of Colorado, Boulder, CO
Specimen preparation and final assembly performed at the Laboratory for Atmospheric and Space Physics, University of Colorado, Boulder, CO

See 2.2.2 for test cell description.

Test Cell ID#2 was used for the .189 psid F2 flight experiment on the MGM-II mission.

3.2.5 HW5 – MGM Test Cell ID#H

PI-provided.
Built by Sandia National Laboratories, Albuquerque, NM and the Laboratory for Atmospheric and Space Physics, University of Colorado, Boulder, CO
Specimen preparation and final assembly performed at the Laboratory for Atmospheric and Space Physics, University of Colorado, Boulder, CO

See 2.2.2 for test cell description.

Test Cell ID#H was used for the .007 psid F3 flight experiment on the MGM-II mission.

3.2.6 HW6 – MGM Test Cell ID#E

PI-provided.
Built by Sandia National Laboratories, Albuquerque, NM and the Laboratory for Atmospheric and Space Physics, University of Colorado, Boulder, CO
Specimen preparation and final assembly performed at the Laboratory for Atmospheric and Space Physics, University of Colorado, Boulder, CO

See 2.2.2 for test cell description.

Test Cell ID#E was used for the .075 psid F3 flight experiment on the MGM-II mission.

3.2.7 HW7 – MGM Test Cell ID#G

PI-provided.
Built by Sandia National Laboratories, Albuquerque, NM and the Laboratory for Atmospheric and Space Physics, University of Colorado, Boulder, CO
Specimen preparation and final assembly performed at the Laboratory for Atmospheric and Space Physics, University of Colorado, Boulder, CO

See 2.2.2 for test cell description.

Test Cell ID#G was used for the .189 psid F3 flight experiment on the MGM-II mission.

3.2.8 HW8 – MGM Accumulator Purge Fittings

PI-provided.
Built by Sandia National Laboratories, Albuquerque, NM

The accumulator purge fittings are used in the deactivation phase of each experiment as part of the procedure to restore the accumulators to their default starting configuration. There are 2 purge fittings, 1 for the water jacket accumulator and 1 for the specimen accumulator. The purge fittings are stowed in the MGM foam-padded lockers, separate from the TDLA and test cells.

3.2.9 HW9 – Drink Bag

PI-provided.

The accumulator purge procedure, which is performed during the deactivation phase of each experiment, expels excess water from the water jacket accumulator. A standard crew drink bag is connected to the purge fitting attached to the water jacket accumulator to collect this water. One drink bag is used for each of the 6 experiments. The drink bags are stowed in the MGM foam-padded lockers, separate from the TDLA.

3.2.10 HW10 – Memory Card

PI-provided.

Intel commercial off-the-shelf item.

For each flight experiment, 2 memory cards are installed in the CEU in Locker 1. The memory cards are redundant; an identical complete set of experiment data is stored on each card. The memory cards provide non-volatile storage for the recorded flight data. A total of 12 memory cards are used. Each card has a capacity of 10 megabytes. The memory cards are stored in the MGM foam-padded lockers and are returned to the lockers after use.

3.2.11 HW11 – Canon L-1 Camcorder

STS-provided.
Canon commercial off-the-shelf item.

For each experiment, the MGM video output is recorded on Hi-8 video tape using an STS-provided camcorder in VCR mode. The MGM video output consists of the signals from the 3 built-in video cameras in Locker 2, multiplexed into a single output signal. The MGM video output and the camcorder are connected via the VIU.

3.2.12 HW12 – Hi-8 Video Tape Cassette

STS-provided.
Commercial off-the-shelf item.

For each experiment, the MGM video output is recorded on one 120-minute Hi-8 video tape cassette.

3.2.13 HW13 – Payload and General Support Computer (PGSC)

STS-provided.
IBM commercial off-the-shelf item.

The PGSC is used by the Mission Specialist to control each MGM experiment. The MGM.exe (version 2.06) software program is pre-loaded on the PGSC hard drive. The PGSC is connected to the PIP mounted on Locker 1 by a serial interface cable.

3.2.14 HW14 – MGM PGSC Floppy Disks

PI-provided.
Commercial off-the-shelf item containing PI-provided software.

The MGM PGSC Floppy Disk contains a backup copy of MGM.exe (version 2.06), the software program used by the Mission Specialist to control the experiments. Two identical disks are provided.

3.2.15 HW15 – PGSC Serial Cable

STS-provided.

The PGSC serial cable is used to connect the PGSC to the serial port on the PIP.

3.2.16 HW16 – MGM PIP-VIU Video Cable

PI-provided.

The MGM PIP-VIU Video Cable is used to connect the VIU to the video output port on the PIP.

3.2.17 HW17 – MGM Bench Test System

PI-provided.

Built by Sandia National Laboratories, Albuquerque, NM

The MGM Bench Test System is used for 1-g ground testing of specimens and as a testbed for experimental techniques and software. The Bench Test System consists of flight-like CEU, accumulators, sensors and plumbing. The plumbing on the Bench Test System is configured horizontally to minimize the effects of water head on confining pressure in the 1-g tests.

3.2.18 HW18 – MGM Test Cell ID#i

PI-provided.
Built by Sandia National Laboratories, Albuquerque, NM and the Laboratory for Atmospheric and Space Physics, University of Colorado, Boulder, CO
Specimen preparation and final assembly performed at the Laboratory for Atmospheric and Space Physics, University of Colorado, Boulder, CO

See 2.2.2 for test cell description.

Test Cell ID#i was reserved as a flight spare and used in anomaly testing following the flight.

3.2.19 HW19 – MGM Test Cell ID#9

PI-provided.
Built by Sandia National Laboratories, Albuquerque, NM and the Laboratory for Atmospheric and Space Physics, University of Colorado, Boulder, CO
Specimen preparation and final assembly performed at the Laboratory for Atmospheric and Space Physics, University of Colorado, Boulder, CO

See 2.2.2 for test cell description.

Test Cell ID#9 was reserved as a flight spare and stabilized in its original, undeformed state following the flight.

3.2.20 HW20 – Space Acceleration Measurement System (SAMS)

NASA-provided.

The SAMS equipment provides a record of the acceleration environment in which the MGM experiments are performed. The data recorded by this equipment is retrieved electronically from Lewis Research Center (LeRC) after the flight, and is used in the MGM data analysis.

3.3 Sessions/Functional Objectives (FO) Table

Mission	Session Name	FO#	HW#	Scheduled day	Actual day	Samples/Parameters	Method
STS-89	Specimen Preparation	2, 3	HW2, HW3, HW4, HW5, HW6, HW7, HW18, HW19	L - 45 start	10/30/97 - 11/11/97		Specimen Prep. (2.4.1)
STS-89	Experiment 1	1, 2, 4, 5	HW1, HW2, HW8-HW13	FD 2 1/24/98	FD 2 1/24/98	Confining pressure 0.007 psid	F2 Quasi-static axial compression (2.4.2)
STS-89	Experiment 2	1, 2, 4, 5	HW1, HW3, HW8-HW13	FD 4 1/25/98	FD 4 1/25/98	Confining pressure 0.075 psid	F2 Quasi-static axial compression (2.4.2)
STS-89	Experiment 3	1, 2, 4, 5	HW1, HW4, HW8-HW13	FD 5 1/26/98	FD 5 1/26/98	Confining pressure 0.189 psid	F2 Quasi-static axial compression (2.4.2)
STS-89	Experiment 4	1, 2, 4, 5	HW1, HW5, HW8-HW13	FD 6 1/27/98	FD 7 1/28/98	Confining pressure 0.007 psid	F3 Cyclic axial compression (2.4.2)
STS-89	Experiment 5	1, 2, 4, 5	HW1, HW6, HW8-HW13	FD 7 1/28/98	FD 8 1/30/98	Confining pressure 0.075 psid	F3 Cyclic axial compression (2.4.2)
STS-89	Experiment 6	1, 2, 4, 5	HW1, HW7, HW8-HW13	FD 8 1/30/98	FD 9 1/30/98	Confining pressure 0.189 psid	F3 Cyclic axial compression (2.4.2)
STS-89	Experiments 1, 2, 3, 4, 5, 6	6	HW17	FD2, FD4, FD5, FD6, FD7, FD8	FD2, FD4, FD5, FD7, FD8, FD9	SAMS head 3, 25 Hz bandwidth	SAMS data acquisition (2.4.3)
STS-89	CT scanning	7,8	HW2-7, HW19	R + 7 weeks	3/16/98		CT scanning (2.4.4)
STS-89	Flight spare specimen stabilization	9, 10	HW16	R + 13 weeks	6/18/98		Epoxy impregnation (2.4.5)
STS-89	Specimen 4 stabilization	9, 10	HW5	R + 14 weeks	6/24/98		Epoxy impregnation (2.4.5)
STS-89	Specimen 5 stabilization	9, 10	HW6	R + 15 weeks	7/3/98		Epoxy impregnation (2.4.5)

Table 2. Sessions/Functional Objectives (FO), MGM-II, STS-89.

Mission	Session Name	FO#	HW#	Scheduled day	Actual day	Samples/Parameters	Method
STS-89	Specimen 6 stabilization	9, 10	HW7	R + 16 weeks	7/20/98		Epoxy impregnation (2.4.5)
STS-89	Specimen 3 stabilization	9, 10	HW4	R + 17 weeks	Scheduled 7/29/98		Epoxy impregnation (2.4.5)
STS-89	Specimen 2 stabilization	9, 10	HW3	R + 18 weeks	Scheduled 8/5/98		Epoxy impregnation (2.4.5)
STS-89	Specimen 1 stabilization	9, 10	HW2	R + 19 weeks	Scheduled 8/12/98		Epoxy impregnation (2.4.5)

Table 2 (cont.). Sessions/Functional Objectives (FO), MGM-II, STS-89.

4.4 Discussion of Method/Protocol

4.4.1 Specimen Preparation (Pre-flight)

In order to perform identical tests during flight, identical specimens were needed. Due to the nature of the material and preparation technique, slight differences between specimens are unavoidable. The steps taken to minimize these differences are described below.

Test specimens were prepared at the Laboratory for Atmospheric and Space Physics (LASP) at University of Colorado at Boulder, using F-75 Ottawa sand placed by dry pluviation. Each specimen was weighed and diameter measurements were taken, and relative density was calculated. Once calculations confirmed that specimen preparation was satisfactory, the test cells were assembled and pressurized to 15 psig.

The cells were then observed until delivery, with minor maintenance performed. Periodic repressurization was performed to account for any relaxation of cell materials, and cell and specimen integrity was monitored. Relaxation was minimal, and largely took place within the first day after initial pressurization, and thus was successfully dealt with by repressurization.

4.4.1.1 STS-79 Specimens

During the observation period, one bellows in test cell ID#3 showed leakage. Water was entering the bellows slowly, thus the bellows would have eventually become inoperable. Also, test cell ID#7 was drained and refilled 8/12/96, exchanging the previously vibrated load cell with an unvibrated one, in response to concerns of the integrity of vibrated load cells. All other cells contained unvibrated load cells.

Five test specimens were built in preparation for STS-79 flight testing. Table 3 lists preparation and usage information for the five specimens. Three specimens were chosen for flight, taking the most uniform specimens with closest relative density and most favorable long-term behavior. The remaining two specimens were set aside for use as flight spares, if required. As the spare test cells were not used for flight, they were dedicated as control specimens. One was used for a ground truth test; the other was left undisturbed. All five were stabilized by epoxy impregnation following the flight.

HW#	Test Cell ID#	Preparation Date	Relative Density	Comments
HW2	0	8/13/96	87.3%	0.007 psi Test
HW3	4	6/19/96	85.9%	0.075 psi Test
HW4	7	6/17/96	86.4%	0.189 psi Test
HW15	2	6/19/96	85.9%	Ground Truth Test
HW16	3	6/18/96	84.3%	Undisturbed

Table 3. Summary of Specimen Preparation for STS-79.

4.4.1.2 STS-89 Specimens

During observation, one bellows in test cell ID#2 showed leakage. Water was entering the caged bellows slowly, thus the bellows would have eventually become inoperable. The motor on test cell ID#G replaced 1/8/98 in response to concerns of movement of the motor housing. The load cell in test cell #9 was replaced 12/22/97 after developing a large offset.

Eight test specimens were built in preparation for flight testing, with four designated for the F2 series tests, and four designated for the F3 series tests. The only operational difference between the F2 and F3 test cells was the gear ratio on the compression motor. Table 4 lists preparation and usage information for the eight specimens. Six specimens were chosen for flight, three of the F2 and three of the F3 test cells, taking the most uniform specimens with closest relative density and most favorable long-term behavior. The remaining two specimens were set aside for use as flight spares, if required. As the spare test cells were not used for flight, they were dedicated as control specimens. One was used for post-flight anomaly at the SPPF; the other was left undisturbed. After the flight, the six flight specimens and the undisturbed specimen were scanned at KSC Computed Tomography System and are undergoing stabilization by epoxy impregnation.

HW#	Test Cell ID#	Preparation Date	Relative Density	Comments
HW2	0	11/10/97	64.8%	0.007 psi F2 Test
HW3	1	10/30/97	62.2%	0.075 psi F2 Test
HW4	2	11/11/97	65.0%	0.189 psi F2 Test
HW5	H	11/08/97	66.7%	0.007 psi F3 Test
HW6	E	11/02/97	66.3%	0.075 psi F3 Test
HW7	G	11/03/97	66.0%	0.189 psi F3 Test
HW18	i	11/08/97	67.3%	Anomaly Testing
HW19	9	11/01/97	62.3%	Undisturbed

Table 4. Summary of Specimen Preparation for STS-89.

4.4.2 Flight Experiments (In-Flight)

Each of the three F1 and three F2 flight experiments was performed using an axial, quasi-static, relatively large magnitude cyclic displacement loading mode. The loading sequence consisted of 5 displacements (compressions) of 5% axial strain each separated by unloading cycles, for a total axial strain of 25%. The displacement rate during loading was 35 mm/hr. The displacement rate during unloading was 17.5 mm/hr.

Each of the three F3 flight experiments was performed using an axial, quasi-static, small magnitude cyclic displacement loading mode. The loading sequence was comprised of 10 small cycles and 7 larger cycles. Each of the ten small cycles consisted of a 0.5 mm compression followed by a 0.5 mm

extension. Each of the seven larger cycles consisted of a 5 mm compression followed by a 5 mm extension. The displacement rate during the small cycles was 35 mm/hr. The displacement rate during the larger cycles was 75 mm/hr.

The 3 F1 experiments were performed on 3 identical test cells, using the same experiment sequence each time. The confining pressure was set at 0.007 psid for STS-79 Experiment 1, at 0.075 psid for STS-79 Experiment 2, and at 0.189 psid for STS-79 Experiment 3. The 3 F2 experiments were performed on 3 identical test cells, using the same experiment sequence each time. The confining pressure was set at 0.007 psid for STS-89 Experiment 1, at 0.075 psid for STS-89 Experiment 2, and at 0.189 psid for STS-89 Experiment 3. The 3 F3 experiments were performed on 3 identical test cells, using the same experiment sequence each time. The confining pressure was set at 0.007 psid for STS-89 Experiment 4, at 0.075 psid for STS-89 Experiment 5, and at 0.189 psid for STS-89 Experiment 6. Confining pressure was closely controlled throughout the experiments.

4.4.3 SAMS Data Collection (In-Flight)

The Space Acceleration Measurement System (SAMS), sponsored in support of microgravity science experiments by the NASA Microgravity Science and Applications Division, recorded the acceleration environment during MGM experiments with triaxial sensors. For MGM-I on STS-79 the C sensor head was mounted near the TDLA on the forward SPACEHAB bulkhead. MGM-II experiments on STS-89 were performed in the TDLA mounted on the aft bulkhead with sensor heads A and B located nearby to record accelerations. The frequency response of the sensor heads was 0.01 to 25 Hz.

The post-flight archived SAMS data are available through the Principal Investigator Microgravity Services (PIMS) at NASA Lewis Research Center. The SAMS data were downloaded from the PIMS server for the time periods of active operation (power on) of the three MGM flight experiments. The data, consisting of acceleration “g” values in the X-, Y-, and Z-axes of the various sensors, referred to STS coordinates as a function of mission time, were examined to determine deviations from +/- 1 milli-g (mg) requirements for each experiment data set.

4.4.4 Specimen Computed Tomography Scanning (Post-Flight)

The nine flight specimens and the two undeformed flight spare specimens underwent computed tomography scans at the Kennedy Space Center Computed Tomography System. The scanning generates two-dimensional images of slices perpendicular to a specimen’s cylindrical axis which may be combined electronically to generate volumetric data sets that allow analysis of internal features. The CT scanning method substantially enhances the science by allowing observation of internal features and provide a guide for cutting specimens in preparation for internal examination.

The process was performed on 4 specimens at one time, and took cross-axial scans at 1 mm intervals over the length of the specimen.

4.4.5 Specimen Stabilization (Post-Flight)

The 9 flight specimens and the two undeformed flight spare specimens were Stabilization by epoxy impregnation to permit evaluation by classical thin-sectioning techniques. Introduction of epoxy into the specimens and subsequent curing and hardening stabilized the sand grains against

disturbance. This allows safe handling of the specimens and dissection by saw-cutting and preparation of thick and thin sections that will be analyzed to assess specimen fabric and pore structure.

The epoxy impregnation was performed with a 4 part epoxy mix that was low in viscosity and well suited for saw cutting, grinding and polishing in preparation of thin sections. To facilitate the internal analysis, two dyes were incorporated into the epoxy to enhance contrast in both reflected and transmitted illumination during microscopic examination. After thorough mixing the dyed epoxy was introduced into the bottom of the specimen by gravity feed. By adjusting the level of liquid epoxy in the feed vessel the flow rate upward into and through the specimen was controlled within predetermined limits that would ensure no disturbance of particles. After the specimen was completely filled with epoxy the specimen was placed in a 70°C oven and cured for 16 hours.

5 Results

5.1 Anomalies

5.1.1 STS-79 Anomalies

5.1.1.1 Pre-flight Anomalies

5.1.1.1.1 Load Cell Sealing

Description of Anomaly
Each MGM test cell contains a load cell which provides a reading of the load applied to the specimen during compression. The load cell readings are an important science data item. Sandia National Laboratories procured 12 load cells in 1994 from M/D Totco, Inc.; these load cells were intended to be sufficient for all flight and ground experiments.

During ground testing the MGM team discovered that 3 of the load cells displayed large shifts in their output. The load cell housing is an aluminum canister, with aluminum end caps sealed with epoxy. Investigation by the load cell manufacturer revealed that the cause of the shifts was water which had leaked into the load cells through cracks in the epoxy. The water caused internal shorting of the Wheatstone bridge strain gauge, which biased the output of the load cell.

Each of the failed load cells had been vibrated during MGM qualification testing. Not all vibrated load cells exhibited failures. None of the unvibrated load cells exhibited failures. The manufacturer concluded that the seal cracking was caused by vibration. In all 3 cases the failure was slow to appear following vibration: the shortest time between vibration and evidence of failure was five months.

Resolution of Anomaly
For the flight test cells, the MGM team selected load cells which had never been vibrated. The failure history of the load cells indicated that water leakage into the cracked load cells was extremely slow. If a crack developed in the epoxy seal during launch vibration it was unlikely to lead to failure of the load cell before the experiments were performed. In addition, actual launch vibration levels were predicted to be lower than the qualification vibration levels which had led to failures.

Effect on Science Return
No failures appeared during or after the flight. This anomaly had no effect on the science return.

5.1.1.2 In-Flight Anomalies

5.1.1.2.1 Experiment 1 Water Venting During Deactivation

Description of Anomaly
During the deactivation phase of Experiment 1, to help alleviate a tight schedule caused by delays in other crew activities, the MGM team agreed to halt the experiment deactivation procedure as early as possible without loss of science data, and to write a new procedure for completing the deactivation later.

The anomaly occurred during execution of the new deactivation procedure. During a step which should have lowered pressure in the MGM system to 14.7 psia, the water jacket accumulator motor ran opposite of the expected direction, causing the pressure in the water jacket system to increase. The pressure relief valves functioned properly and a small amount of water was vented into MGM Locker 1 before the procedure was halted. The Mission Specialist performing the procedure (Carl Walz) cleaned up the water without incident.

Resolution of Anomaly
The MGM team created a work-around procedure that successfully completed deactivation later that day. Post-flight investigation of the anomaly showed that it was due to the omission of a step in writing the new deactivation procedure. The MGM team omitted the execution of a user-interface "Stop Motors" command which was believed to be superfluous under the circumstances. This omission was in error, and caused the anomaly. To avoid a recurrence of this anomaly on subsequent flights, the importance of this command has been emphasized to the MGM team.

Effect on Science Return
This anomaly had no effect on the science return. The anomaly occurred after the test cell had been returned to storage pressure and disconnected from the water jacket accumulator.

5.1.1.2.2 Experiment 3 Absolute Pressure Sensor Sensitivity

Description of Anomaly
During the deactivation phase of Experiment 3, the water jacket absolute pressure sensor was seen to be producing erroneous readings. The sensor readings fluctuated by 5 - 10 psi in response to very small (± 0.005 psi) changes in the actual pressure. The system depends on these readings during experiment deactivation to control the two-step process in which the pressure in the test cells is raised from the test pressure first to 0.5 psid, then to the storage pressure of 15 psid. While the system was able to raise the test cell pressure properly, the fluctuations in the sensor readings made it difficult for the system to determine success and terminate the process.

Resolution of Anomaly
The process was terminated manually with a software command. At the time of termination the test cell had been returned to its final, stable storage condition. The remaining steps in the deactivation procedure configure the TDLA for the following experiment. Since this experiment was the final MGM experiment of the mission, the MGM team decided to terminate the deactivation phase at that point.

Post-flight examination of the data shows that this sensor was producing erroneous readings throughout the experiment, although the readings had no effect on the experiment until the deactivation phase.

The MGM team tested this sensor after landing, prior to removing the MGM experiment hardware from the SPACEHAB module. During that testing the sensor performed nominally: all readings were stable and correct. Following the return of the MGM flight hardware to UCB/LASP, a fault tree was generated and the sensor was subjected to a thorough program of exercises and tests, both while installed in the TDLA and by itself on the bench. The MGM team was unable to reproduce the failure, or to identify any other source of the erroneous sensor readings. The sensor manufacturer (Lucas

Schaevitz) was not able to suggest additional tests or causes of failure other than those in the fault tree.

The MGM team replaced this sensor with a spare for the next mission.

Effect on Science Return
Since the system was able to successfully return the test cell to storage pressure, and since the anomaly occurred at the end of the final experiment, there was no effect on the science return from the mission.

5.1.1.3 Post-flight Anomalies

5.1.1.3.1 TDLA Grounding

Description of Anomaly
During post-flight testing, McDonnell Douglas/SPACEHAB personnel performed measurements indicating that the TDLA violated the single-point grounding scheme for the orbiter 28V power. Measurements at UCB/LASP confirmed this. The orbiter 28V return and orbiter chassis ground were connected in the MGM electronics. The cause was design error, rather than assembly error or malfunction. The verification inspection procedure performed at delivery did not include a check for this condition.

Resolution of Anomaly
The PIP was reworked to enforce the required single-point grounding scheme for the next mission.

Effect on Science Return
This anomaly caused no apparent effect on science return. All 3 flight experiments were performed under the same conditions.

5.1.2 STS-89 Anomalies

5.1.2.1 Pre-flight Anomalies

There were no pre-flight anomalies.

5.1.2.2 In-Flight Anomalies

5.1.2.2.1 Absolute Pressure Sensor Sensitivity

Description of Anomaly
The water jacket absolute pressure sensor was producing erroneous readings. The sensor readings fluctuated by 5 - 10 psi in response to very small (± 0.005 psi) changes in the actual pressure. The system depends on these readings during experiment activation to control the two-step process in which the pressure in the test cells is lowered from storage pressure of 15 psid to 0.5 psid and also during the deactivation to control the two-step process in which the pressure in the test cells is raised from the test pressure first to 0.5 psid, then to the storage pressure of 15 psid. While the system was able to lower and raise the test cell pressure properly, the fluctuations in the sensor readings made it difficult for the system to determine success and terminate the process.

This anomaly began in Experiment 4. During post-flight analysis of the data stored in the memory cards, however, the investigators found an anomaly in

the engineering sensor records: these records were apparently not correctly stored during the first minutes following power-on. No anomalies were found later in the records, and there was no loss of science data.

The anomaly was detected during the activation phase of Experiment 4, as confining pressure was being lowered from the storage pressure of 103 kPa (15 psig) to 3.5 kPa (0.5 psig) under software control, Mission Specialist J. Reilly observed that the system seemed to be oscillating around the desired pressure. The MGM team advised Reilly to halt the automatic sequence, then continue with the rest of the activation phase and the proceeding experiment using contingency operating procedures which used manual motor-movement commands to raise and lower pressures during activation and shutdown portions of the experiment.

Although the pressure sensor anomaly that appeared in Experiment 4 continued in Experiment 5 and Experiment 6, the contingency operating procedures allowed the experiments to run with no loss of science data.

Resolution of Anomaly

The MGM team concluded that the oscillation was due to a recurrence of an anomaly that first appeared on the MGM-I mission. The symptom of this anomaly is that the coarse pressure sensor on the water side of the experiment fluid system appears hypersensitive, responding to small changes in actual pressure with large fluctuations in the reported pressure reading. When the pressure in the system is stable, the sensor produces stable, accurate readings. Troubleshooting efforts following the MGM-I mission failed to reproduce the anomaly, and its cause was not determined. To prepare for the MGM-II mission the pressure sensor was replaced with a spare, and the MGM team prepared contingency operating procedures which do not depend on stable readings from this sensor. These procedures allowed the experiment to be completed with no loss of science data.

The MGM team tested this sensor after landing, prior to removing the MGM experiment hardware from the SPACEHAB module. During that testing the sensor performed nominally: all readings were stable and correct.

The MGM flight hardware was transported to MSFC, and the sensor was subjected to a program of exercises and tests while installed in the TDLA. The source of the anomaly has been identified to be a Symmetrics quick-disconnect (QD) assembly. The sensor, which is connected on the plumbing between the water jacket accumulator and the QD connecting the plumbing to the test cell, senses momentary increases in pressure when the accumulator is moved. The increase is sensed because the QD provides too much of a constriction to flow. The exact cause of the constriction has not been determined, but is known to be related to the small filter screens inside the QDs which are intended to prevent any objects in the test cell (such as a sand grain) from entering the plumbing and the accumulator. The filter screens may be too small or becoming clogged, preventing water from freely flowing into the test cell when the accumulator is moved.

The MGM team plans to correct the problem with the QDs by means such as altering the current 10-micron size screens to a larger mesh which would still protect the plumbing and accumulator, but also allow better flow. A decision will be made at the completion of further testing which is including flow tests involving the QD and is aimed at isolating the source of the problem and the best method to prevent the reoccurrence.

Effect on Science Return
Since the system was able to be successfully operated using the contingency procedure, there was no effect on the science return from the mission.

5.1.2.2.2 Memory Card Recording Discrepancies

Description of Anomaly

For each experiment, science and engineering data are recorded on two memory cards which create a duplicate set that contains the same information on each card. After return of the memory cards to the PI, the data was examined and it was detected that the memory card sets were not exact duplicates. During five of the experiments (Experiment 2 excluded) the sets had a number of instances where the engineering data was not the same on the two cards. Post flight testing showed that the anomaly was caused by incomplete erasure of some of the memory cards.

Resolution of Anomaly

For future missions all flight memory cards will be erased and checked before launch.

Effect on Science Return

Since the errors were found only in sections of the memory cards which record engineering data, there was no loss of science return from the mission.

5.1.3.2 Post-flight Anomalies

There were no post-flight anomalies.

5.2 Completeness/Quality of Data

5.2.1 Completeness of Data Return

For complete success the MGM experiment plan required the retrieval of 9 sets of data from each experiment (F1, F2, F3): the digital data stored in memory cards, the video tape recorded from the 3 flight cameras, and the test cell containing the deformed specimen. All 6 data sets from each of the three flight experiments were successfully retrieved. There was no loss of science data from any cause; all records are complete.

The amount of stored digital data from the 9 experiments is approximately 75 megabytes. Since the experiment stores a redundant copy of all data for each experiment in a second memory card, the total amount of data returned was approximately 150 megabytes. The data has been read from the memory cards and processed using software developed by the MGM team.

The video data consist of nine 120-minute Hi-8 tapes, one tape from each experiment. Each tape contains the three views provided by the three built-in cameras, multiplexed at 1-second intervals. This data has been re-recorded for viewing and analysis.

The three STS-79 flight test cells underwent optical profile measurements at Marshall Space Flight Center (MSFC). The measurements are a record of the final external contours of the deformed specimens, and will aid in calibration

of the video data. The raw data volume from these optical profile measurements is approximately 100 megabytes.

The three STS-79 and six STS-89 test cells were returned to UCB/LASP, where they were stabilized by epoxy impregnation. The two STS-79 flight spare test cells, which had been prepared using the same procedures as the three test cells actually chosen for flight, were also stabilized by epoxy impregnation: one in the fully compressed state and one in the undeformed state. The STS-89 undeformed flight spare was also stabilized.

The three STS-79 specimens, as well as the two flight spares were delivered to the Non-Destructive Testing and Evaluation (NDT&E) facility at Los Alamos National Laboratory (LANL) for cross-axial CT scanning at high resolution in slices spaced at 1 millimeter intervals results in 115-120 images per specimen. Scanning of each F1 specimen produces approximately 230 megabytes of data for a total of 1.15 gigabytes.

The three STS-79 and six STS-89 test cells and undeformed flight spare test cell were later delivered to the KSC Computed Tomography System where cross-axial scanning was performed at 1 mm intervals, summing to 126 slices for the F1 specimens, 120 for the F2 specimens, and 153 for the F3 specimens and the undeformed flight spare. Resolution for the scans was 0.387 mm/pixel. Scanning of each F1 and F2 specimen produces approximately 35 megabytes of data. Scanning of each F3 and undeformed specimen data produces approximately 43.7 megabytes worth of data for a total of 420 megabytes.

5.2.2 Quality of Data Return

Sample Dryness/Cohesion Prevention

To meet mission requirements, MGM test cells must withstand storage periods of several months. Because of this, diffusion of water from the water jacket into the membrane and granular material has been studied. Diffusion is a concern because moisture can cause apparent cohesion between the granular material particles. To minimize water transfer, latex membranes with a thickness of 0.012 inch and a coefficient of permeability on the order of 10^{-14} cm/sec were used.

Table 5 summarizes diffusion records for five specimens. Diffusion of water into both the granular material and membrane was minimal. Moisture in flight specimens was not directly measured, as specimens underwent epoxy impregnation post-flight. However, previous diffusion records show that granular material samples took on a maximum of 1.60 grams of water during a six-month storage test: a critical moisture level would have been over ten times this amount. Flight specimens were stored for only three months. During preparation for epoxy injection, the top and bottom of each specimen were exposed, and the granular material appeared to have remained dry.

The attempt to keep flight specimens dry appears to have been successful. The result of such a success is minimal cohesion due to moisture in the specimen.

Test Location	Start Date	End Date	Water Weight		Sand	
			Membrane	Sand	Water Content	Saturation
SNL	12/22/94	1/17/95	1.00	0.00	0%	0%
SNL	1/17/95	2/15/95	1.20	0.24	0.022%	0.11%
SNL	2/17/95	7/11/95	1.00	1.60	0.15%	0.70%
LASP	2/16/95	5/10/95	2.20	1.46	0.13%	0.64%
LASP	5/12/95	6/12/95	0.70	0.90	0.082%	0.40%

Table 5. Summary of Diffusion Record for MGM.

5.2.3 Quality of Test Performance

Basic information may be seen in load-displacement and volume displacement curves (Figures 1 to 9, 12) which indicate the flight tests ran properly and that reasonable data was collected. On both F1 and F2 experiments, the load initially rises in a nearly linear fashion to a peak, after which the load decreases, while the volume continues to increase. This is the general trend seen during a drained triaxial test on a medium-dense granular material during 1-g testing. Loading-unloading behavior is also generally well defined, being governed by elasticity and displaying hysteresis. During testing, specimens went through five loading-unloading cycles. The slopes of the curves during the cycles are similar, and the reloading portion of the curve extends back to the load curve prior to unloading. Another dominant feature is the oscillation in the load throughout all tests. While load-displacement data are very indicative of quality tests, volume measurement also shows that test performance was nominal. A volume increase in all specimens was expected and did occur, during in-flight experiments as well as ground experiments.

On the loading portions of F3 experiments, the load increases in a nearly linear fashion and begins to level out. When unloading begins, the load drops quickly, then becomes fairly level and returning to nearly zero load. In addition, the load required to complete a compression-extension cycle decreases with each cycle.

In summary, several features indicate that all tests ran well and produced reliable data.

6 Discussion

6.1 Overview

Science information is obtained from four types of data: digital (load, pressure, deformation, and volume change of specimens during compression), optical (in-flight video and post-flight profile measurements), CT, and internal examination. SAMS data also indicate whether external accelerations disturbed the experiments.

Digital data collected from several types of transducers during compression are used to study behavior of granular material under load in the low-confining pressure region. F1 experiments (MGM-I, STS-79) were performed on 86.5 ±0.8% relative density specimens, and F2 (MGM-II, STS-89) on 63.6 ± 1.4% relative density specimens. Both F1 and F2 specimens were compressed to large (25%) axial strain, to obtain general static material properties. The third type of test examined 66.4 ± 0.4% relative density specimens under small-strain cyclic loading, to obtain cyclic behavior (for liquefaction applications, etc.): these tests are indicated as F3, and are identical to F2 experiments, with exception of the loading history. Three tests, at confining pressures of 0.007, 0.075, and 0.189 psi were performed on each type of experiment (F1, F2 and F3).

Optical data are important in two areas: support of digital data gathered during compression, and surface analysis. Video data were collected from three CCD cameras (spaced at 120 degrees) providing continuous coverage of the specimens' surface deformations during testing. The video provides shape and diameter information during compression. This is used to study deformation patterns and membrane strain.

Computed tomography (CT) scans were performed at the Non-Destructive Testing and Evaluation facility of Los Alamos National Laboratory (F1 specimens) and at the Kennedy Space Center Computed Tomography System (F1, F2, and F3 specimens) after the compressed specimens were returned to the PI. Additional partially compressed terrestrial specimens were also scanned. Cross-axial scans were obtained at 1 millimeter spacing over the long axis of the specimen. The slices are used to construct 3-dimensional volumetric images of the specimen, and inner features may then be examined by exposing internal planes. While the resolution is not high enough to see individual grains, density information is available. This information reveals the internal features of the specimen and aids in planning for internal examination, which is performed following the stabilization of the specimens by impregnating epoxy into the pores of the material.

Internal examination involves cutting the specimens into thick and thin sections. When viewed under a microscope, these sections allow viewing and measurement of void ratio, particle alignment, and other internal features at a high resolution, as individual particles will be visible.

SAMS data were collected during the mission. The MGM team has examined the data recorded during experiments, when specimens were in unstable states due to the extremely low confining pressures and are susceptible to being disturbed by small accelerations. This information helps locate possible external disturbances to the specimens.

Digital, optical, CT, and internal examination data form the basis of understanding granular material behavior in microgravity. SAMS data reveals

external influences on the experiments. All data are correlated to form a comprehensive picture of the MGM flight experiments.

6.2 Status of Data Analysis

6.2.1 Digital Data

Analysis of digital data is ongoing at UCB. All digital data has been reduced and corrections for known instrument effects have been applied. Further processing includes corrections for non-uniform displacement which will proceed with the availability of optical data information.

6.2.2 Optical Data

Data processing and analysis of optical data, which are performed at UCB and MSFC, is in progress. Algorithms have been developed for data processing analysis for both MGM-I and MGM-II. Optical data has been processed and analyzed for initial state data. Processing of data collected during testing is continuing for MGM-I.

6.2.3 Computed Tomography

All of the data have been acquired, and inspected using volumetric visualization tools. A qualitative look at available data has revealed highly interesting internal structure. Quantitative processing has begun, with calibration of data with density information at 75% completion.

6.2.4 SAMS

SAMS data has been acquired and processed. Analyses involving comparing results with science requirements and performing a low resolution comparison with load and pressure data has been completed for MGM-I and MGM-II.

6.3 Preliminary Research Findings

6.3.1 Digital Data

Preliminary findings in the digital data are related to load, pressure, displacement, and volume. Flight data showing principal stress ratio versus axial strain, and volumetric strain versus axial strain are shown in Figures 1 through 9. Principal stress ratio, the ratio of the axial stress to radial stress, normalizes the axial load over confining pressure which allows direct comparison between tests of different confining pressures.

The F1 and F2 specimens exhibited very high friction angles, within the range of 52 to 64 degrees and 48 to 70 degrees, respectively, which is mainly due to grain interlocking effects, which decreased with confining pressure increase. Higher pressure terrestrial tests performed on the same material show lower friction angles. Figure 10 illustrates this variation with confining pressure, and shows values of friction angle for terrestrial, F1, and F2 tests at relative densities of 65% and 85%. Data points with confining pressures above 1.30 kPa are derived from terrestrial test results, and data points with confining pressures below 1.30 kPa are derived from microgravity experiments. Both terrestrial and microgravity experiments were performed at 1.30 kPa.

Principal stress ratio from F3 experiments has revealed two interesting characteristics. First, stress ratios allow determination of peak internal friction angles, which may be compared to F1 and F2 data (Table 6) The friction

angles from F3 tests show the same trend as F2 tests, but are higher for tests at the 0.05 and 1.30 kPa pressures. Secondly, the stress ratio during first cycles of F3 experiments increases at a greater rate than subsequent cycles.

The unloading-reloading traces in all cases appear to be nearly unaffected by the confining stress level. It is also interesting to observe that the specimens display substantial elastic stiffness, with unloading-reloading moduli in the range of 18 to 28 MPa, 12 to 27 MPa, for F1, and F2 tests, respectively, that do not seem to change even after large axial displacements of 20 to 25% and dilation exceeding 10%. The 0.05 kPa confining pressure experiments show large initial stiffness and substantial strain softening and loss of stability, with peak resistance or strength of σ_1/σ_3= 16.5 for the F1 test and σ_1/σ_3= 31.0 for the F2 test at very small strain (less than 1%). The stress-strain responses for the 0.52 kPa F1 and F2 experiments show similar initial stiffness to the 0.05 kPa test, and a distinct peak strength of σ_1/σ_3= 8.5 for the F1 test at approximately 1% axial strain and σ_1/σ_3= 10.5 for the F2 test at less than 1% axial strain. The strain-softening phase is rather ductile in comparison to the 0.05 kPa tests and appears to be controlled, without any local or global material instability. The response at the residual strength level is very similar to that observed in the 0.05 kPa test, though the level for the F1 0.52 kPa test is visibly lower. The stress-strain response of the 1.30 kPa experiment shows initial stiffness behavior that is very similar to the lower confinement tests, while the stick-slip pattern is more pronounced. The peak strength in these experiments is σ_1/σ_3= 9.0 for the F1 test and σ_1/σ_3= 6.5 for the F2 test. The post-peak strain-softening proceeds at a more ductile rate than the 0.52 kPa tests. The residual levels appear to remain quite stable and do not show visible strength reduction, although the F1 residual strength level stays substantially higher than that of the F2 test. The post-peak residual strengths and near constant-volume (critical state) friction angles, shown in Table 7 are in the range of 31° to 40° similar to those observed in terrestrial laboratories, which are typically in the range of 32° to 34° for quartz sand (Bolton, 1986). The effect of the stretched membrane on the radial confining stress has been included in the analysis.

The observed angles of internal friction are unusually large for a granular soil with similar initial densities (Bolton, 1986). The properties for the same material at the same densities, tested at 13.8 kPa and 34.5 kPa gives angles in the range of 44° to 45° for F1 density and 44° to 48° for the F2 density. There is a significant difference between the observed strength behavior at low and high stress levels. In the 0.05 kPa test we observe that the peak strength in F1 is visibly lower than that seen in F2, although the initial density for the F1 test is 20% higher than that of the F2 test. The same pattern appears for the 2 (F1 and F2) 0.52 kPa tests, while the behavior of the 1.30 kPa tests seems consistent with theory. It appears that the relatively higher degree of mobilized resistance in the low confining stress experiments is a result of substantially different deformation mechanisms within the granular fabric, where more work-intensive modes of deformation perhaps involving extensive rotations and sliding occur rather than simple sliding, thus absorbing more of the externally provided energy. The high friction angles do not seem to be attributed to over-consolidation effects.

The Young's moduli observed in the unloading and reloading traces of the experiments are shown in Table 8. All specimens display substantial initial stiffness and elastic moduli during unloading and reloading events, which are nearly an order of magnitude higher than conventional theories predict.

An interesting characteristic of the load cell data of the F1 and F2 experiments is evident in the stress-strain traces (Figures 1 to 6). They are

characterized by distinct periodic oscillations in stress of similar frequency, amplitude and pattern in each experiment, as inelastic deformations dominate the overall responses. All six experiments exhibit oscillations in the principal stress ratio-axial strain (load-displacement) line trace, though to varying extents. In the F1 experiments, the amplitude of the oscillations increases with confining pressure, being more pronounced in the 1.30 kPa test (Figure 3). Also, while the oscillations for all three experiments appear to be of a similar nature, the slip phase of the 1.30 kPa experiment appears to be steeper and to involve greater local instabilities than the other two. In the F2 experiments, the oscillations are more prominent in the 0.05 and 1.30 kPa experiments (Figures 4, 6), and nearly indistinguishable in the 0.52 kPa test (Figure 5). This oscillation in load is also seen in ground testing, to a small extent. This oscillatory behavior is to a large extent attributed to periodic instabilities, which appear to result from buckling and degradation of multiple discrete internal arches and columnar systems (Jaeger et al., 1996a, 1996b). These mechanisms appear to be significantly suppressed in terrestrial (1 gravity) experiments at higher confining stress levels.

Volumetric change is of interest as well, as F1 and F2 specimens show a large amount of dilation, much greater than seen in ground testing. Specimens show very little to no volume decrease at start of test, moving almost immediately into volumetric expansion. The rate of expansion prior to reaching peak loads is dramatically higher than post-peak expansion. Figures 1 to 6 show volumetric strain vs. axial strain response diagrams for the F1 and F2 experiments. The initial responses appear to be very similar for the experiments with initial dilatancy angles in the range of 27 to 31 degrees (see Table 9). Figure 11 illustrates the variation with confining pressure, and shows values of dilatancy angle for terrestrial, F1, and F2 tests at relative densities of 65% and 85%. Data points with confining pressures above 1.30 kPa are derived from terrestrial test results, and data points with confining pressures below 1.30 kPa are derived from microgravity experiments. Both terrestrial and microgravity experiments were performed at 1.30 kPa. There appears to be a significant departure from the initial and nearly linear volumetric expansion at the 4 to 5% axial strain level, where the rate of expansion seems to be reduced by a factor of almost five, resulting in an average dilatancy angle of 3° to 4°, which remains almost constant to the end of the experiments. None of the specimens displayed external evidence of major shear-band formation or other forms of localized deformation. The volumetric changes were generally uniform, with extensive but diffuse bulging at large axial strain levels. The unloading-reloading response traces show pronounced dilatancy during both unloading and reloading stages although the responses also indicate significant elastic behavior, which is seen to a far lesser extent in experiments conducted at high confining stress levels. The volumetric unloading-reloading cycles show very similar stiffness modulus behavior and insignificant relationship between either deformation level or effective confining pressure. In all six experiments the initial stiffness moduli are similar to the unloading-reloading moduli. Based on the difference in the volumetric responses at axial strains before and after approximately 4%, it appears that very different deformation mechanisms are involved. Secondary sets of shear bands form at regular spacings, where dilation in these bands results in additional increases in volumetric strain rather than leveling of the volumetric vs. axial strain traces. This may explain the relatively high residual strength levels.

Volumetric data from F3 experiments are also important. There is a large volume increase in the first cycle, but on subsequent cycles, the net volume change is very little. The initial increase in volume indicates that critical void ratio occurs at the relative densities less than 65%. This is also indicated by the

large volume increase in F1 and F2 specimens: At the conclusion of the tests, the volume had not leveled out, indicating that a true critical state was not achieved. However, it is apparent that critical state must exist at some density less than the lowest density achieved, 4% relative density, which occurred on the F2 specimen tested at 1.30 kPa. As a result, it is apparent that medium-dense cohesionless soil under low confining pressures will not liquefy. This evidence supports the observation that in-situ liquefaction does not occur at the soil surface, where confining pressures are generally low.

In order to study the internal consistency of the experimental findings, boundary (including membrane) effects, and to enhance our understanding of overall specimen behavior nonlinear three-dimensional finite element analyses of the specimen-membrane-end platen system were conducted. Figure 12 shows a composite diagram of the experimental and finite element analyses of the three load-displacement responses, where the membrane effect is included and not corrected. The details of the analyses and the constitutive model and parameters used are described by Jeremic (1997). The correspondence between the experiments and the analyses, using a consistent set of material parameters, which were obtained from separate experiments, show that the findings are reasonable and show internal consistency.

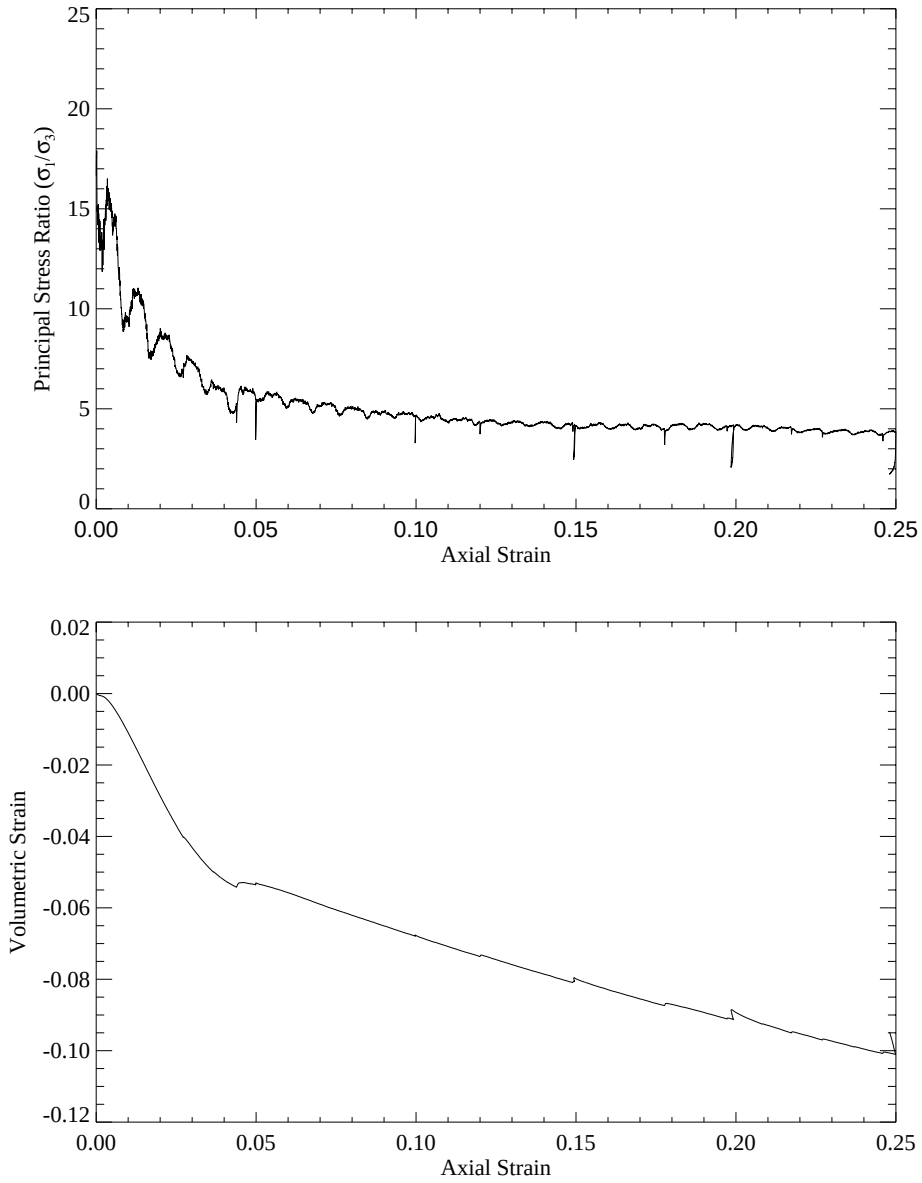

Figure 1. Stress ratio and volumetric strain versus axial strain for the F1 0.05 kPa experiment.

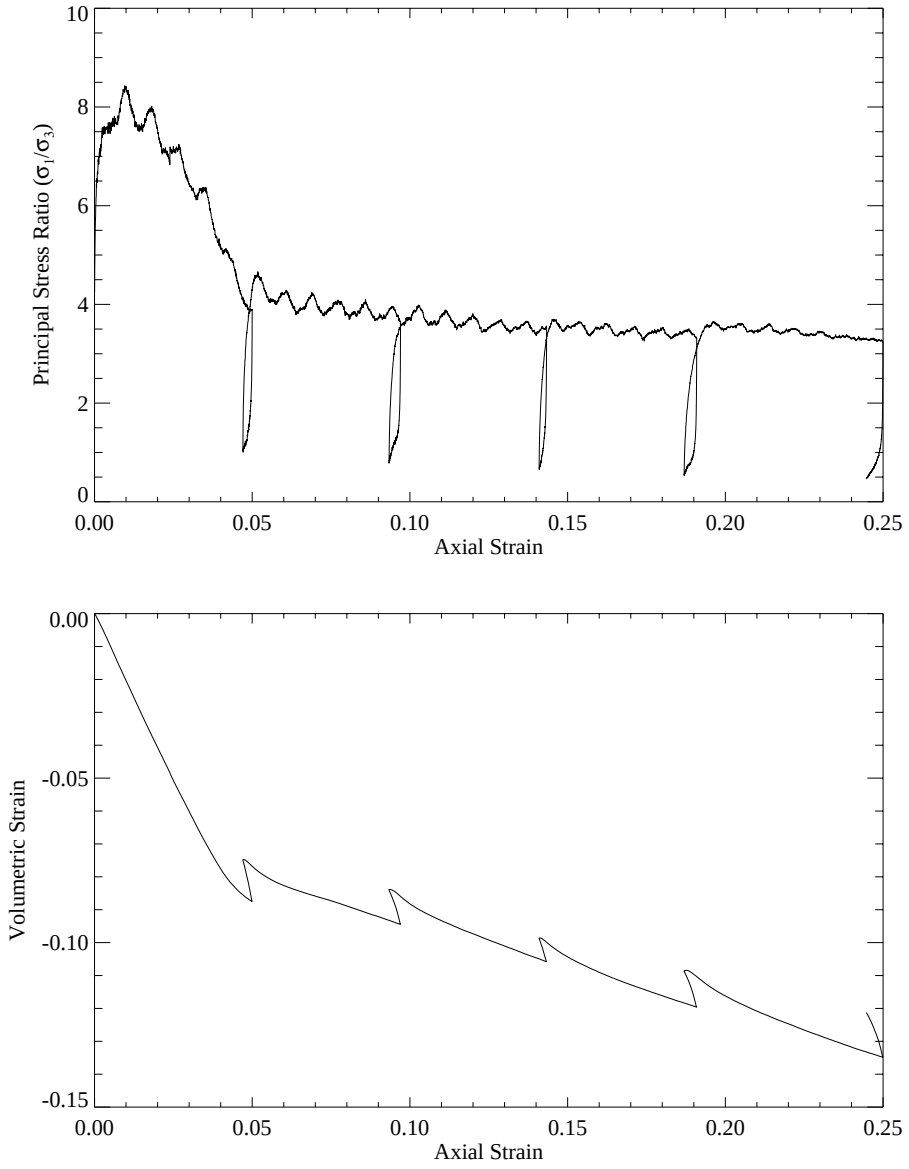

Figure 2. Stress ratio and volumetric strain versus axial strain for the F1 0.52 kPa experiment.

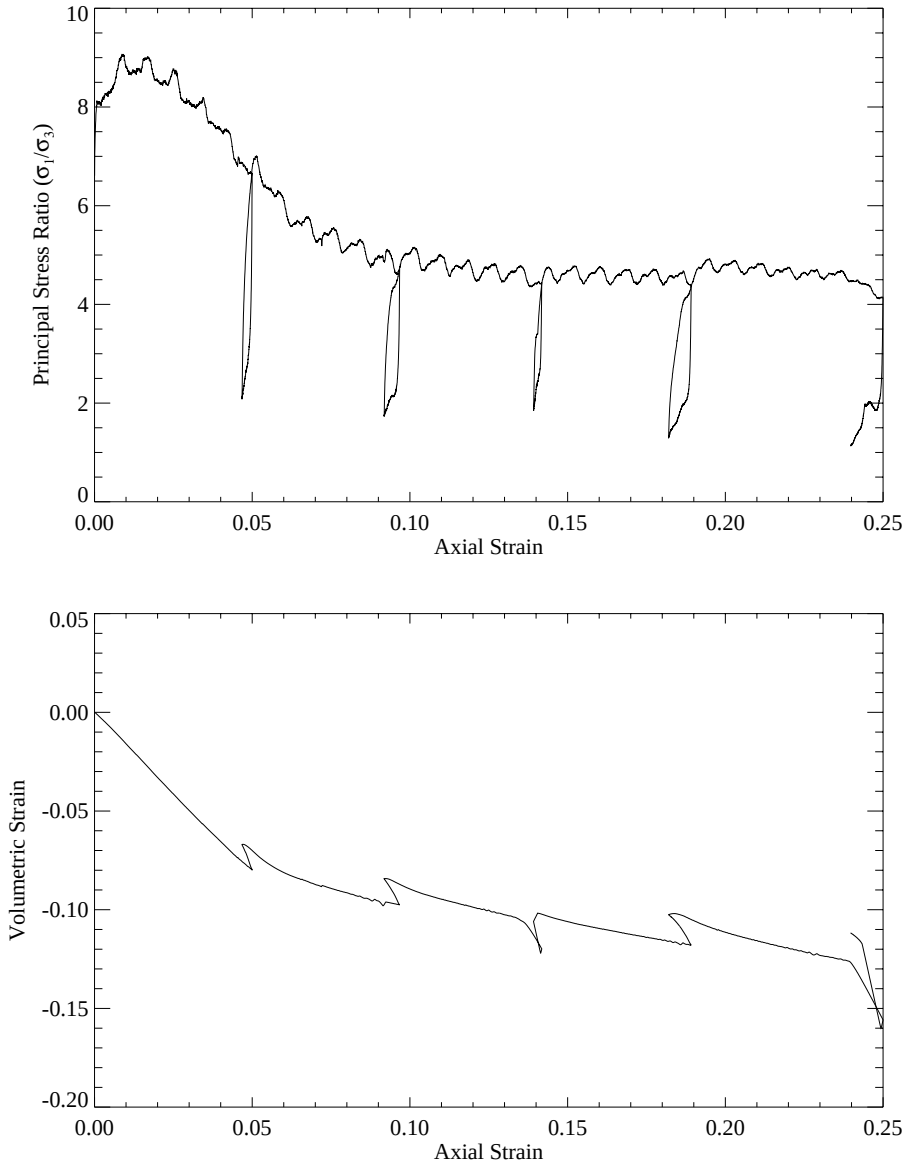

Figure 3. Stress ratio and volumetric strain versus axial strain for the F1 1.30 kPa experiment.

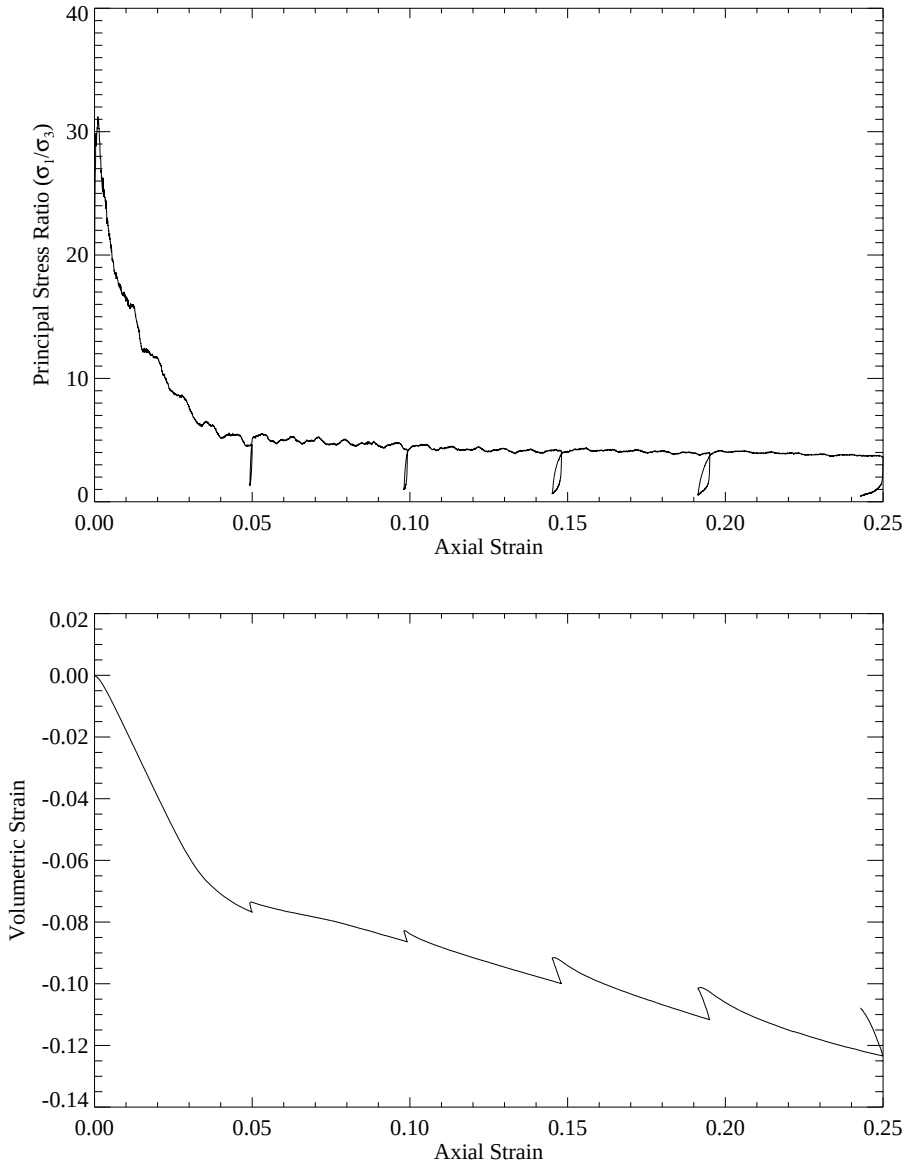

Figure 4. Stress ratio and volumetric strain versus axial strain for the F2 0.05 kPa experiment.

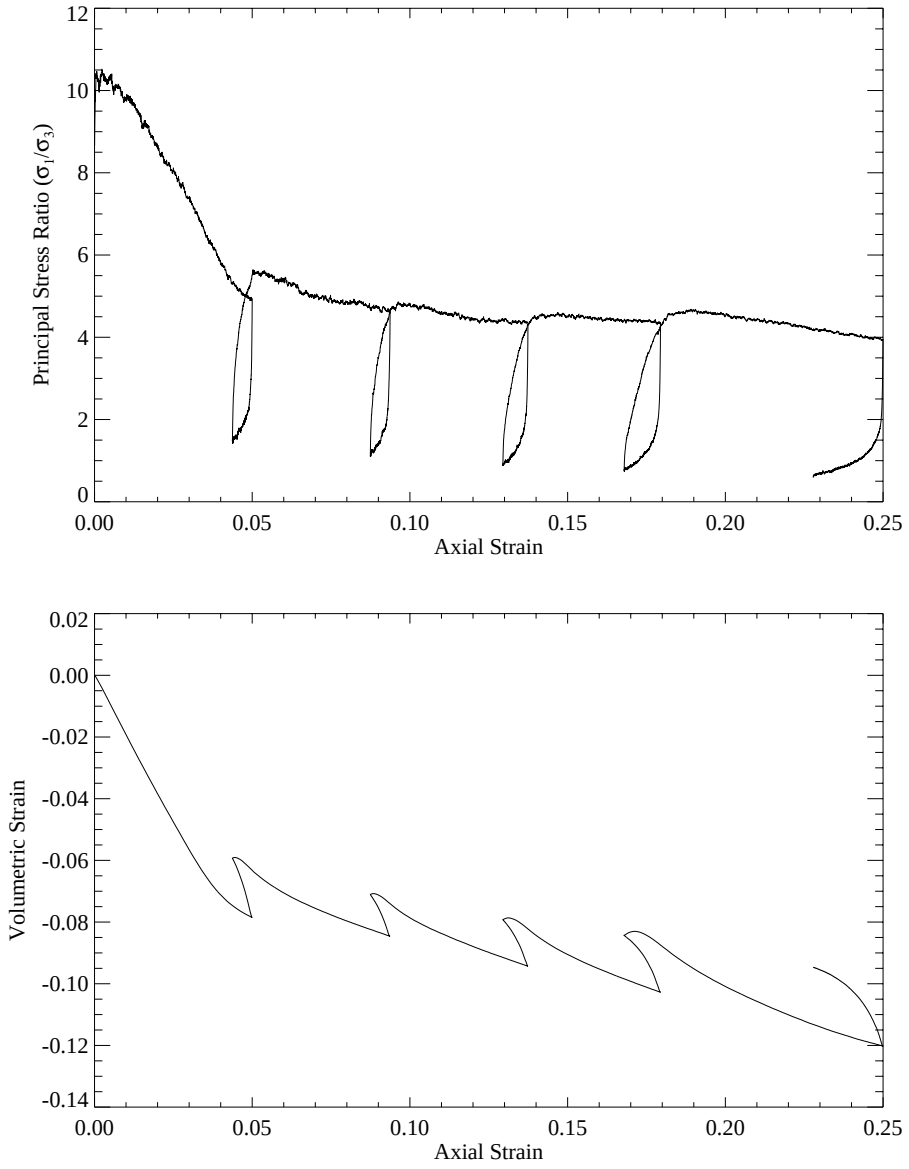

Figure 5. Stress ratio and volumetric strain versus axial strain for the F2 0.52 kPa experiment.

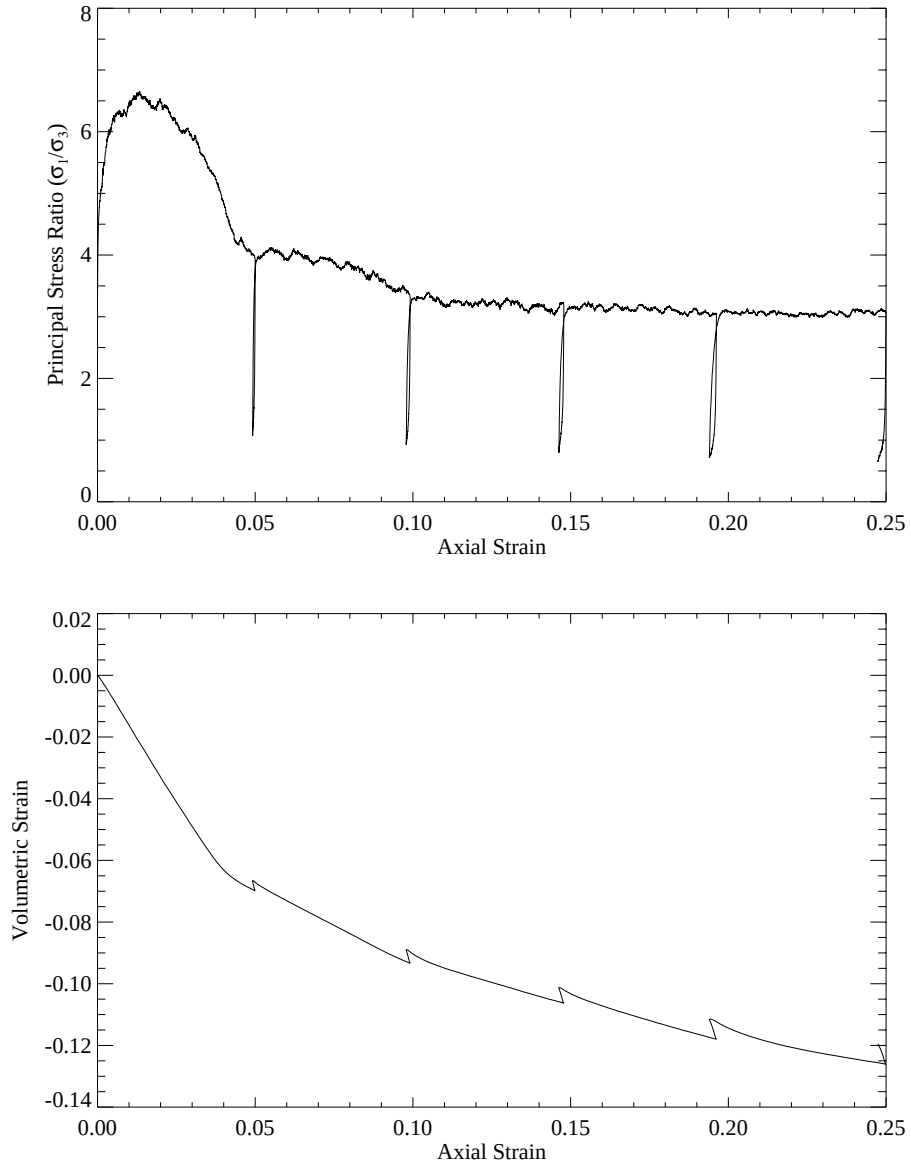

Figure 6. Stress ratio and volumetric strain versus axial strain for the F2 1.30 kPa experiment.

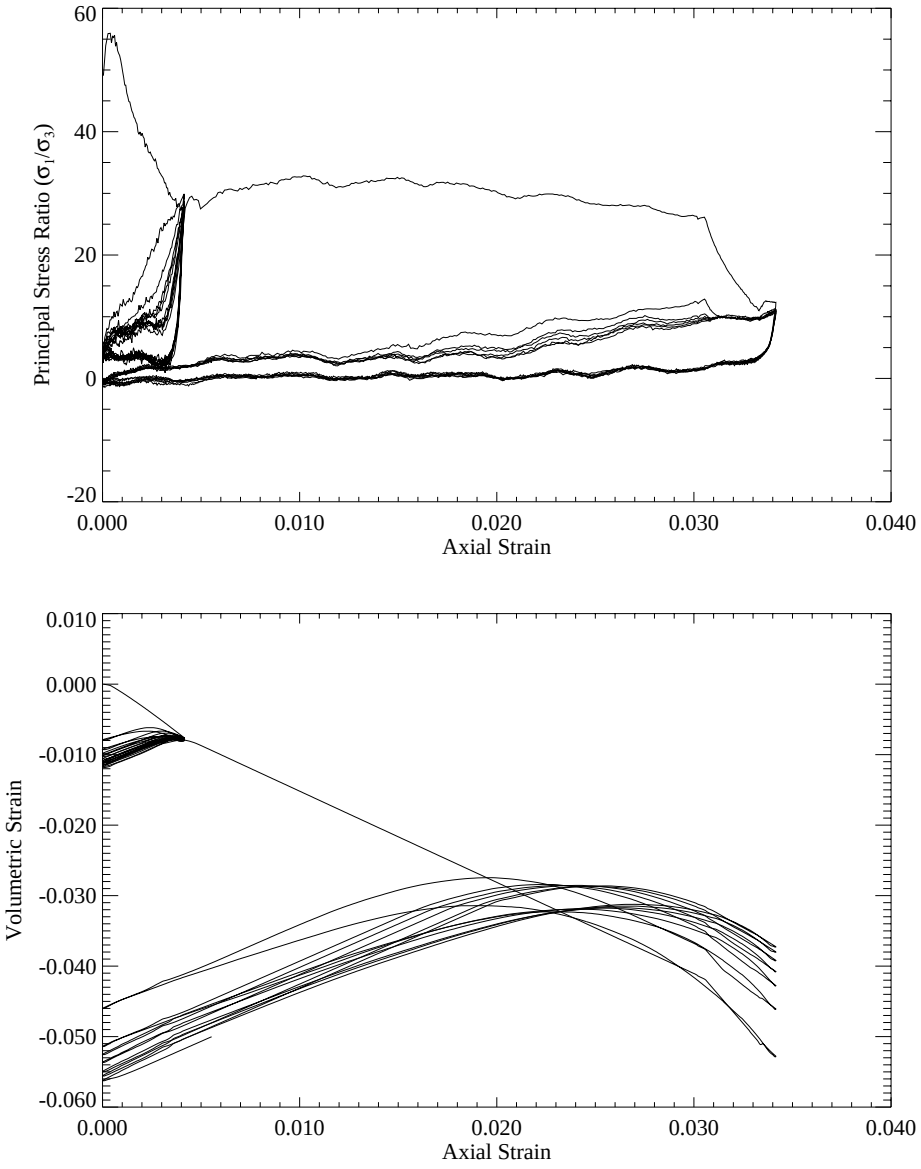

Figure 7. Stress ratio and volumetric strain versus axial strain for the F3 0.05 kPa experiment.

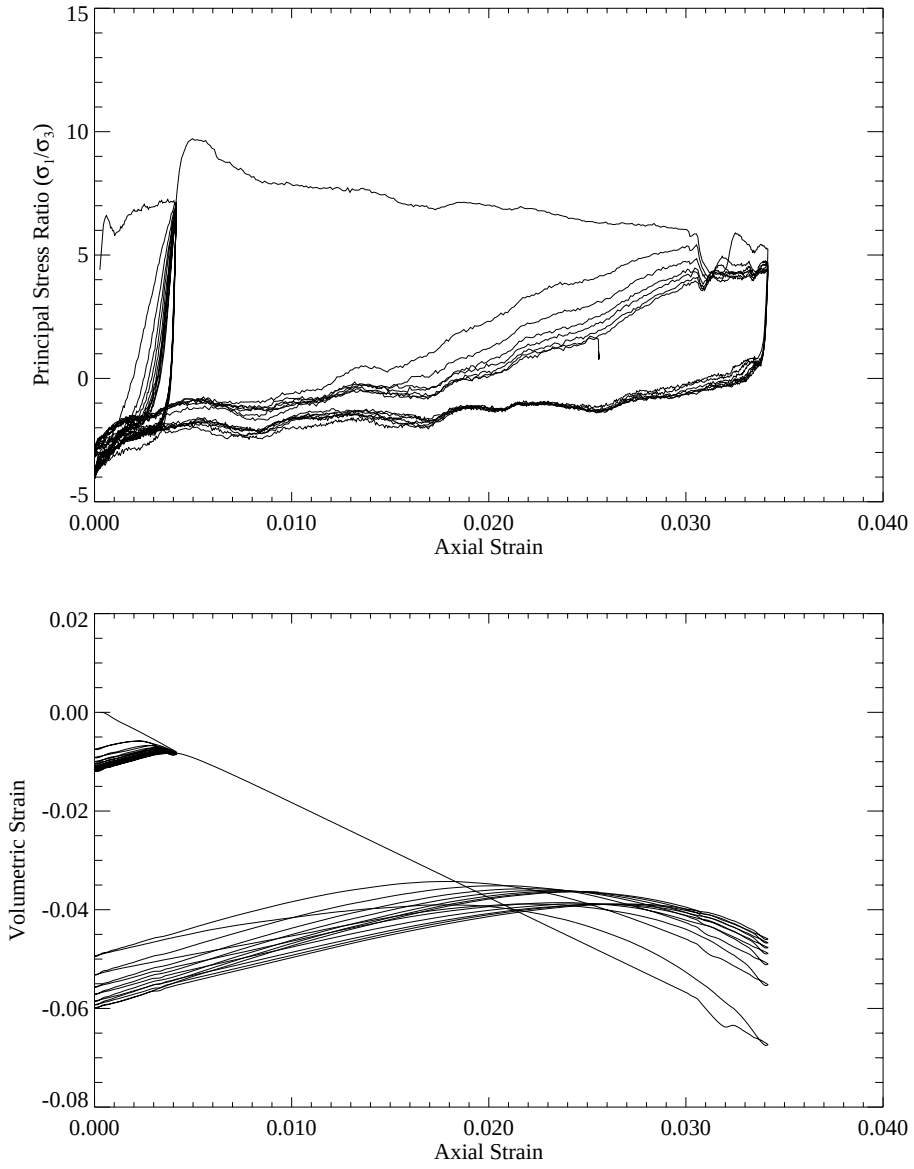

Figure 8. Stress ratio and volumetric strain versus axial strain for the F3 0.52 kPa experiment.

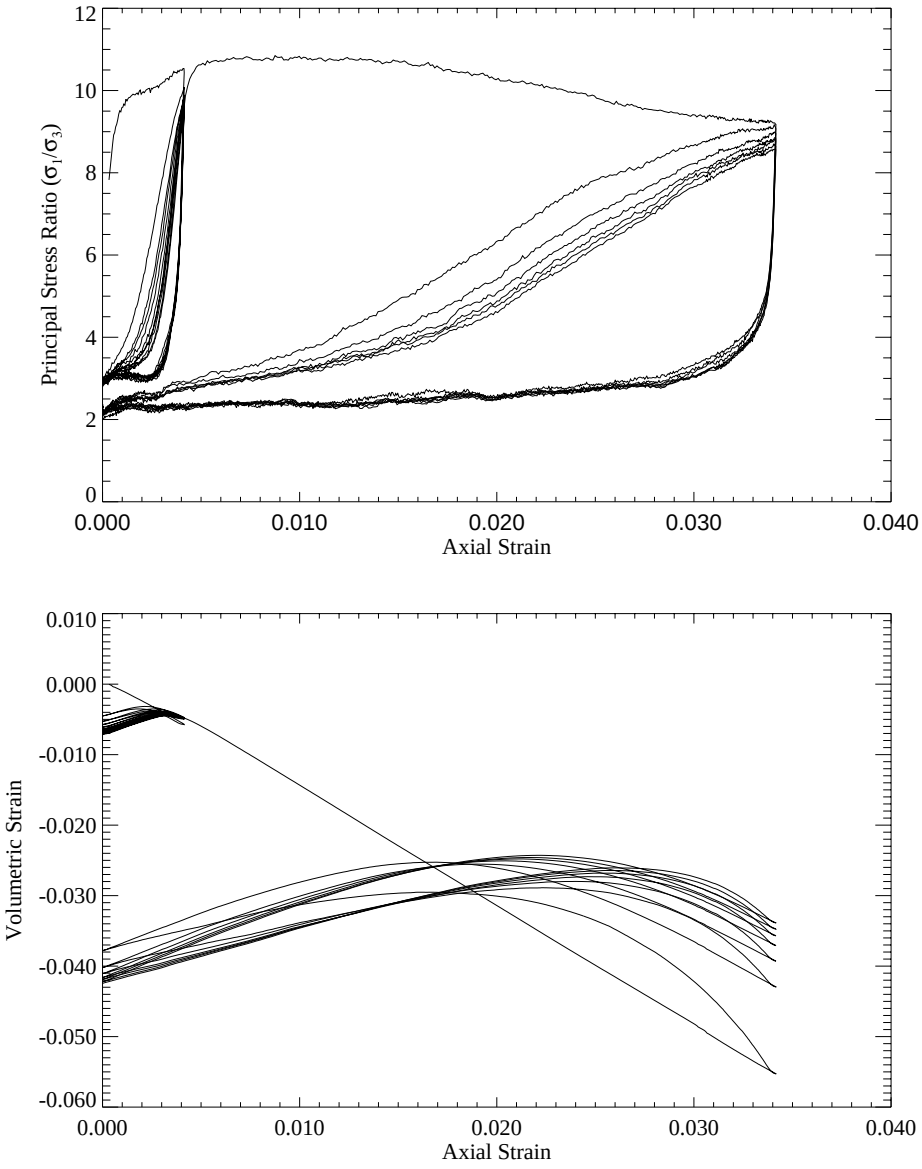

Figure 9. Stress ratio and volumetric strain versus axial strain for the F3 1.30 kPa experiment.

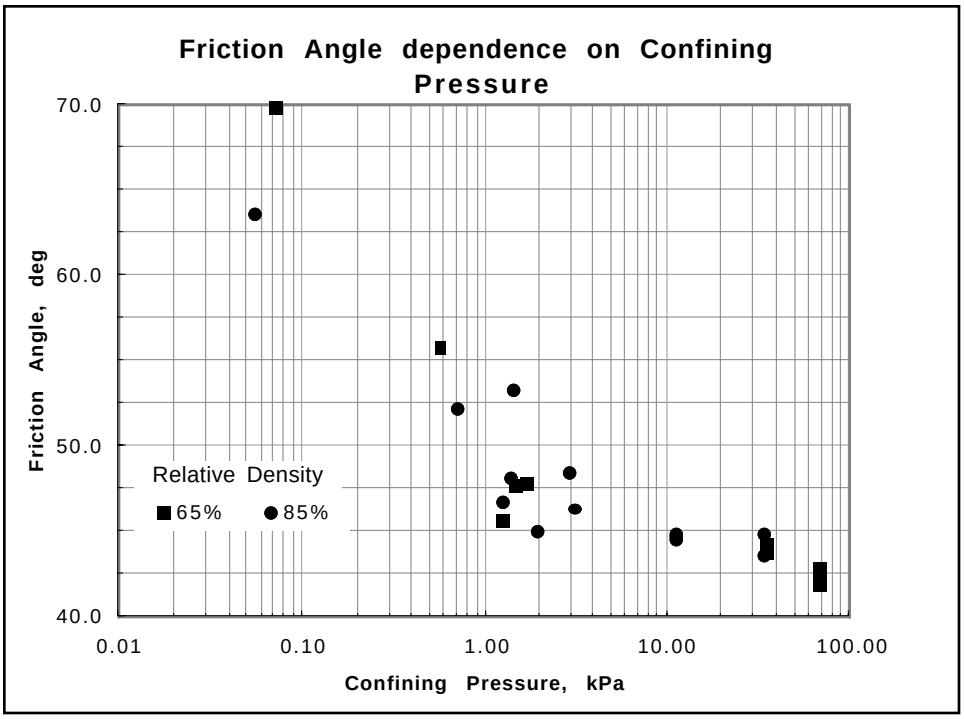

Figure 10. Internal friction angle versus confining pressure.

Nominal Confining Pressure kPa	Peak Internal Friction Angle, deg F1 Tests	F2 Tests	F3 Tests
0.05	64	70	75
0.52	52	55	55
1.30	53	47	56

Table 6. Comparison of peak internal friction angle between F1, F2 and F3 experiments.

Nominal Confining Pressure kPa	Residual Friction Angle, deg F1 Tests	F2 Tests	F3 Tests
0.05	36	37	
0.52	32	35	
1.30	40	31	

Table 7. Comparison of residual/constant volume internal friction angle between F1, F2 and F3 experiments.

Nominal Confining Pressure kPa	Young's Modulus, MPa F1 Tests	F2 Tests	F3 Tests
0.05	5-11	13-27	7-12
0.52	12-19	13-17	18-26
1.30	10-26	24-27	22-27

Table 8. Comparison of Young's Modulus between F1, F2 and F3 experiments.

Nominal Confining Pressure kPa	Dilatancy Angle, deg F1 Tests	F2 Tests
0.05	28	31
0.52	30	29
1.30	27	27

Table 9. Comparison of dilatancy angle between F1 and F2 experiments.

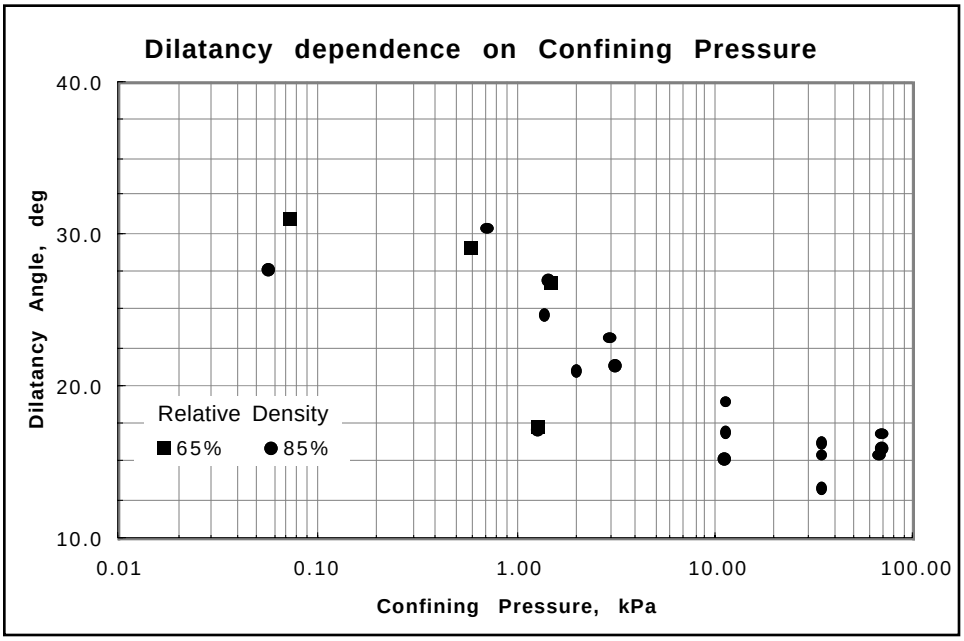

Figure 11. Dilatancy angle versus confining pressure.

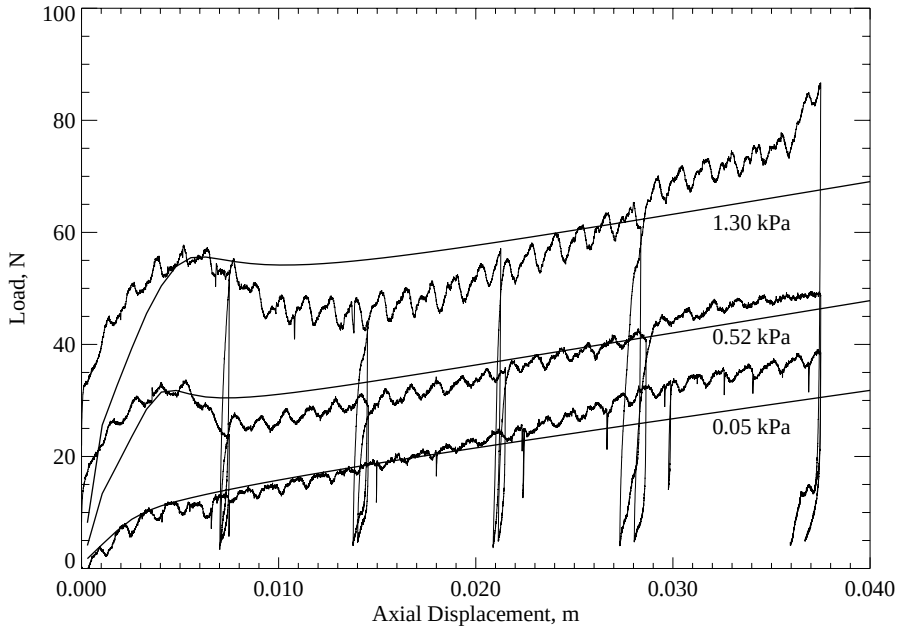

Figure 12. Experimental and finite element analysis of F1 load-displacement responses.

6.3.2 Optical Data

Video data (Figures 13, 14 and 15) reveal deformation characteristics of the flight F1, F2 and F3 specimens, respectively. Specimens did expand radially, as expected. Bulging in the F1 and F2 specimens is also visible, but relatively uniform, revealing a very new phenomenon of diffuse bifurcation instability resulting in overall bulging of the specimen. The small amount of bulging visible in F3 specimens indicates the low friction at the end platens at small strain.

Initial test densities are also been addressed using video data. When specimens were built prior to flight, the height, diameter and mass of the specimen were measured to calculate density. Although the specimens remained intact and cylindrical during launch, the post-launch (pre-test) density may be verified using video data. Video frames from the beginning of each test are grabbed and saved as electronic images. Then, the distortion due to the camera wide-angle lens and the diffraction of the Lexan water jacket and water is corrected. The diameters of the specimen in three locations on each of the three views are measured on the corrected images. This is then combined with the height and mass information taken before launch (as they remain constant) to find a new, post-launch density. These measurements are currently being examined to determine accuracy and precision, as results are heavily dependent on distortion correction and image resolution.

Figure 13. Example video data frame from built-in video cameras, F1 specimen.

Figure 14. Example video data frame from built-in video cameras, F2 specimen.

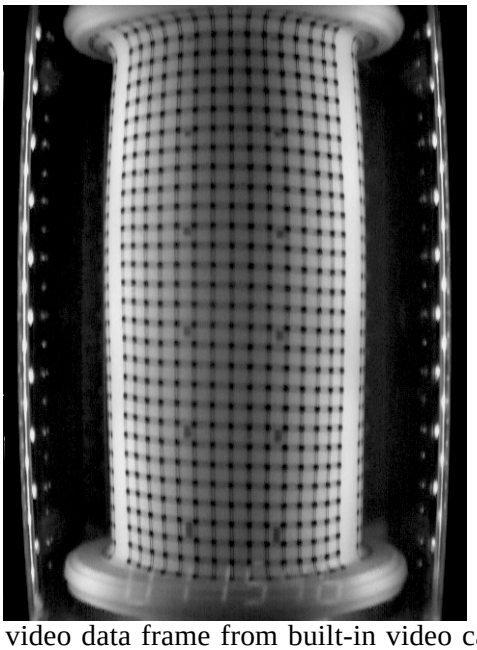

Figure 15. Example video data frame from built-in video cameras, F3 specimen.

Video data recorded by three cameras over the course of an experiment may be used to calculate the geometric shape of a specimen as it evolves over time in response to applied load. Specimen volume and outer surface area are quantified using digitized profile data and known geometry of cameras in relation to the specimen central axis in cylindrical coordinates. Figure 16 shows camera 2 images of the specimen and clock at the beginning of an experiment (left) and 43 minutes later (right) that have been digitized to yield coordinates of boundaries and grid nodes. Figure 17 shows corresponding plots of the digitized coordinates which, when combined with data from the other cameras and suitable interpolation algorithms, allow numerical calculations of specimen volume. The relative displacements of the grid nodes as the specimen deforms give a measure of the surface strain felt by the membrane. In Figure 18 the axial strain derived from the axial grid node displacements of Figure 17 is mapped as contour lines. In a similar manner the lateral strain magnitude and direction were calculated and shown in Figure 19.

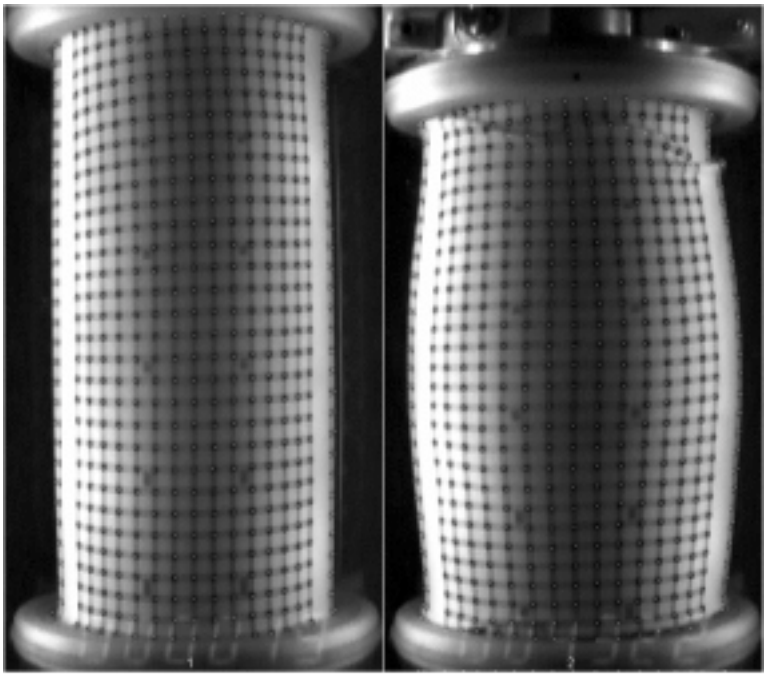

Figure 16. Digitized video frames at beginning and near end of experiment.

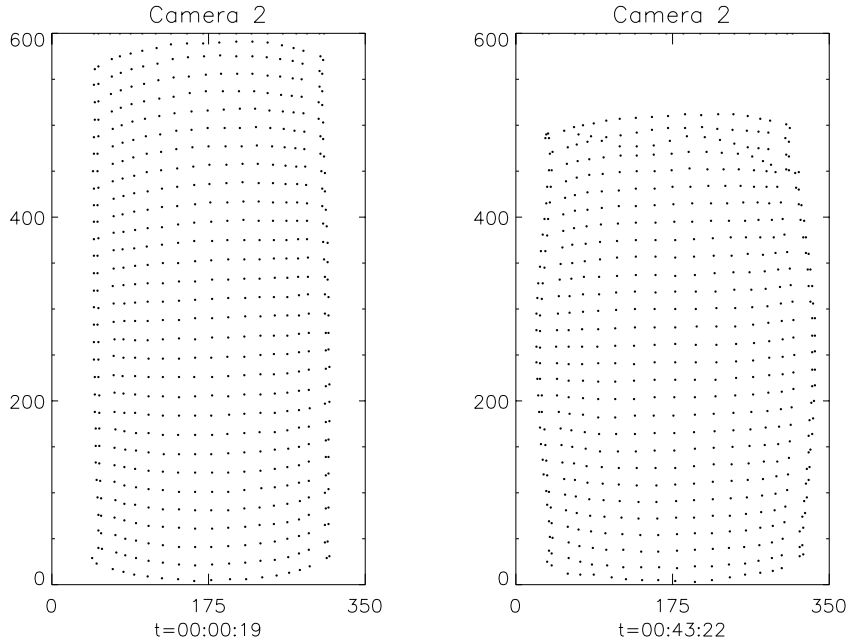

Figure 17. Digitized boundary and grid nodes plotted as pixel coordinates.

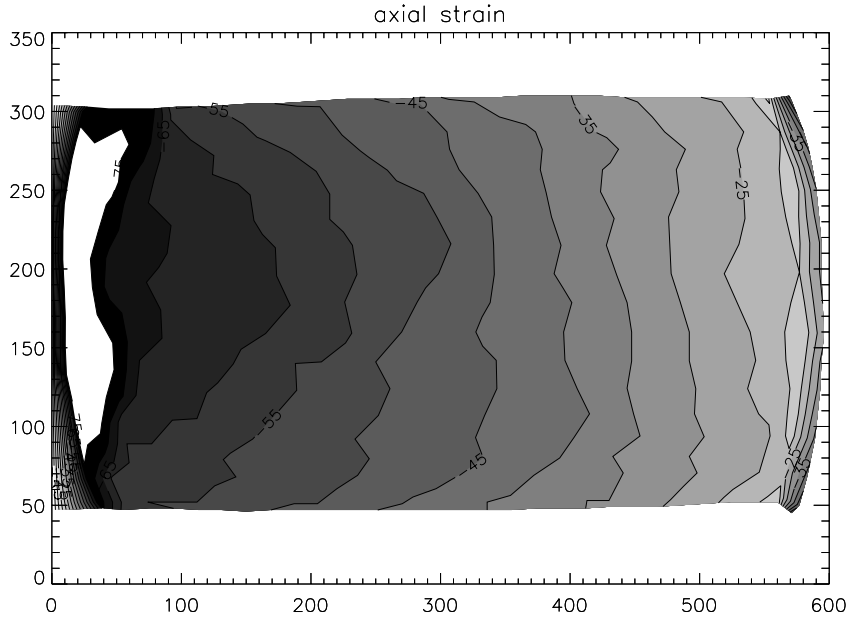

Figure 18. Grid node displacement in axial direction maps axial strain.

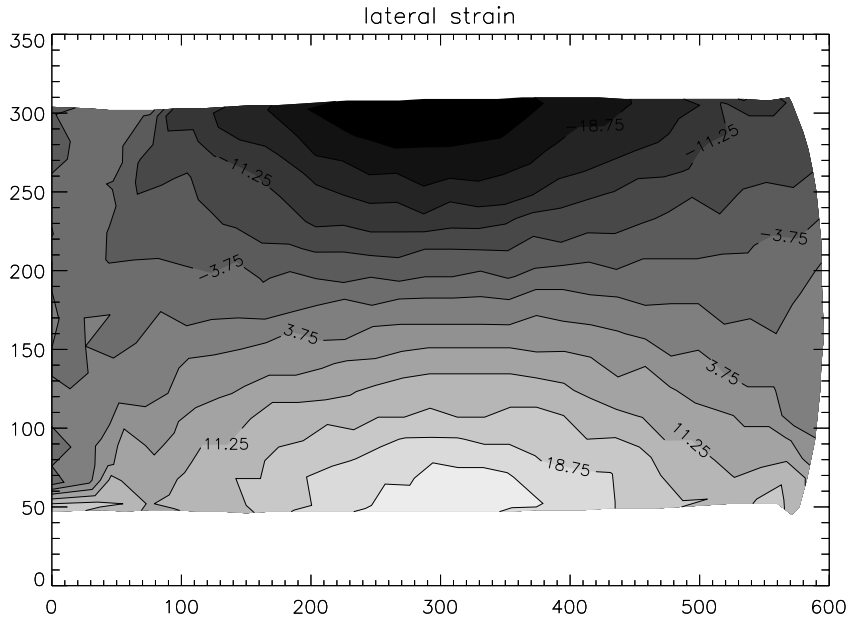

Figure 19. Lateral grid node displacement shows lateral strain.

6.3.3 CT

Figures 20 through 23 show results from CT scans on the F1 and F2 specimens tested at 1.30 kPa. The color bar in the lower right corner of the figure shows an approximate density to color relation, where darker color is

lower density, and lighter color higher density. Cross-sections normal to the axis of compression (Figures 20, 22) show radial regions of lower and higher density areas. A large number of radial discrete bands of lower density, similar in shape to turbine blades mounted on a central hub, extend outward from the boundary of the cones, seen as the central, circular regions. When examining cross-sections parallel with the axis of compression (Figures 21, 23), extensive areas of generally uniform density are seen outside of shear zones. The circular shear cones are seen extending at large angles from each end of the specimens, though the cone on the stationary end platen is more clearly developed. The cones are clearly defined by the specimen-end-platen interface friction and the restraint posed by the stretched latex membrane in the external contact region. Outside of the cones, several inclined lines of low density are identified as the radial bands.

Figures 24 and 25 show results from the CT scan on the F3 specimen tested at 0.05 kPa. Again, the color bar may be used to estimate density. The F3 specimen is much more homogenous than the F1 and F2 specimens (Figures 20 through 23), though small shear cones and beginnings of conjugate shear bands are visible. The shear cone, visible in both the horizontal and vertical slices, is at a very low angle. In contrast, the shear cones visible in F1 and F2 specimens (Figure 21, 23) are steep. This indicates that at the beginning of an experiment, low end-friction is present, and probably increases as the specimen bulges. The conjugate shear bands also indicate that shear band development has begun by 3.3% axial strain in F1 and F2 tests, and that the numerous shear bands visible in F1 and F2 specimens develop throughout the entire test.

Calibration and analysis of the data quality has been performed. First, density calibrations were made on both LANL and KSC data. Calibrations have been compared against bulk density measurements of all specimens. The standard deviation of the void ratio error was 0.017 on the KSC data and 0.050 for the LANL data. It is apparent that the specimens scanned with epoxy embedded in the pores are not calibrated as well as data from specimens scanned prior to epoxy stabilization. Further calibration, particularly of specimens embedded prior to scanning will be required when data is available from thin section microscopic investigations. Measurements have been made to determine the spatial resolution of the data using the modulation transfer function (E1695-95). The KSC data shows 50% modulation at 0.275 line pair per millimeter (lpm), and 10% at 0.53 lpm. The LANL data has approximately twice the resolution, with 50% modulation at 0.55 lpm and 10% at 0.96 lpm (Figures 26, 27.)

CT scans of F1 specimens have been studied, with concentration on void ratio variation within and outside the shear bands. It is apparent that the deformation pattern is dependent on the confining stress, becoming more pronounced as confining pressure increases. F2 and F3 specimens, initially less dense than the F1 specimens, do not show a distinct confining stress dependence on shearing behavior. Measurement of shear band width has also began. Figure 28 shows a cross section of the F1 1g specimen, with several shear bands numbered (10-21) and profile lines indicated by numbers 1-9. Profiles of shear band 10 are shown in Figure 29, where CT number (a measure of attenuation) is plotted against length. From this, the change in density and width of shear bands may be measured. The width of the shear bands range on the order of 8-15 grain diameters, a common value in sand specimens.

To examine the formation of the shear bands, four specimens were compressed to 4.9, 9.4, 12.2 and 16.3 percent axial strain and tomographic

scans produced. Combined with undisturbed samples and specimens compressed to 3.3 and 25% axial strain from F1, F2 and F3 experiments, a progression of internal structure development is obtained (Figure 30.) These data indicate that specimens begin to form a distinctive density pattern as early as 3.3% axial strain, but that shear banding does not fully begin until somewhere between 4.9 and 9.4% axial strain. Many bands are visible at 9.4%, indicating that numerous shear bands form at one time, forming near the shear cone of the move-able end platen and propagating toward the stationary platen.

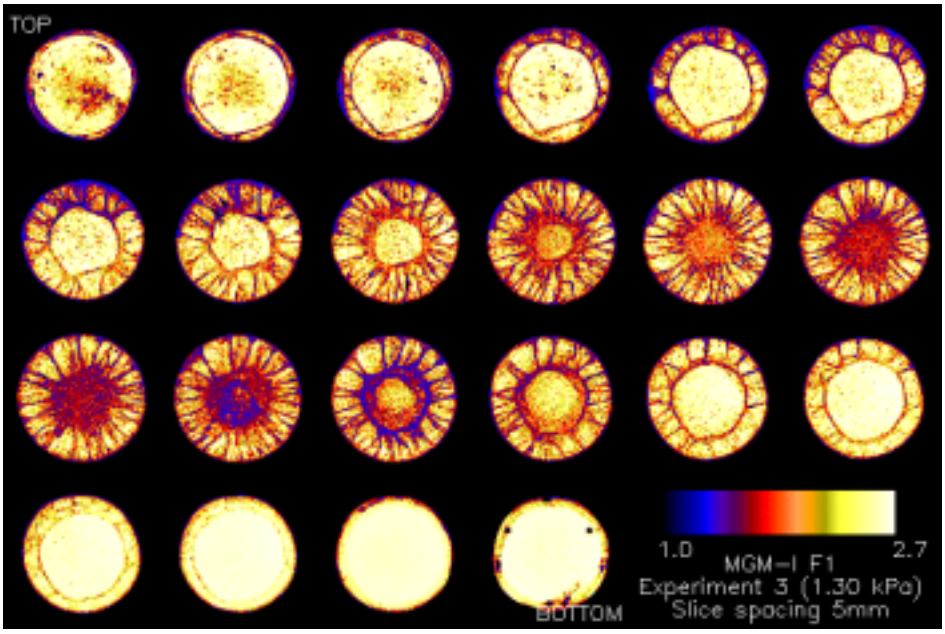

Figure 20. Example of horizontal slices through F1 specimen acquired by CT scanning.

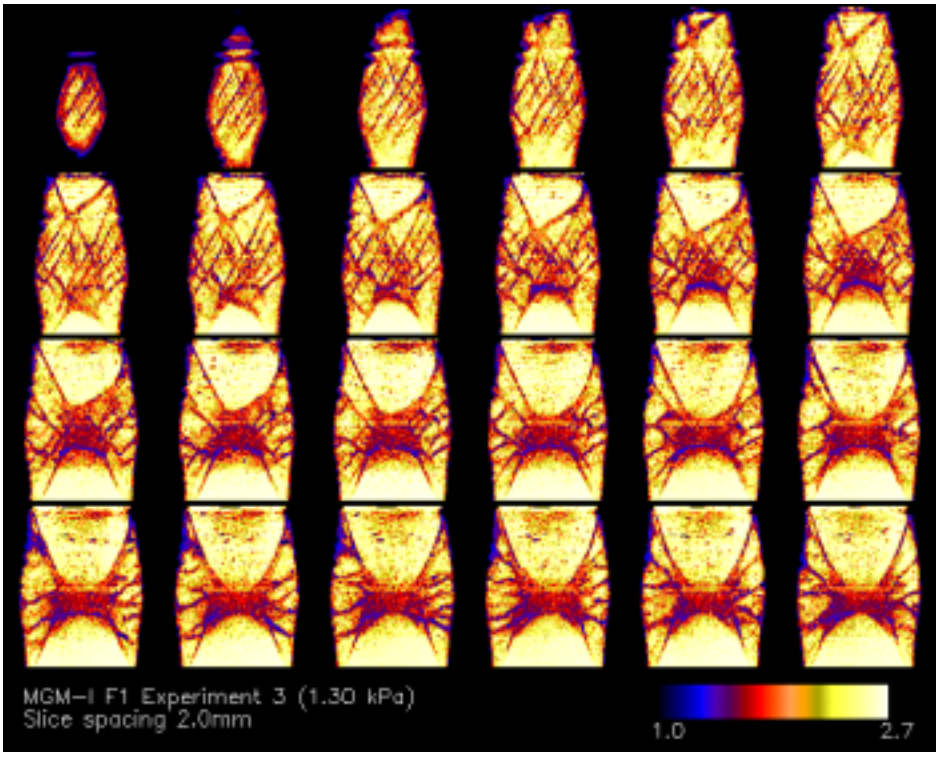

Figure 21. Example of vertical slices through F1 specimen acquired by CT scanning.

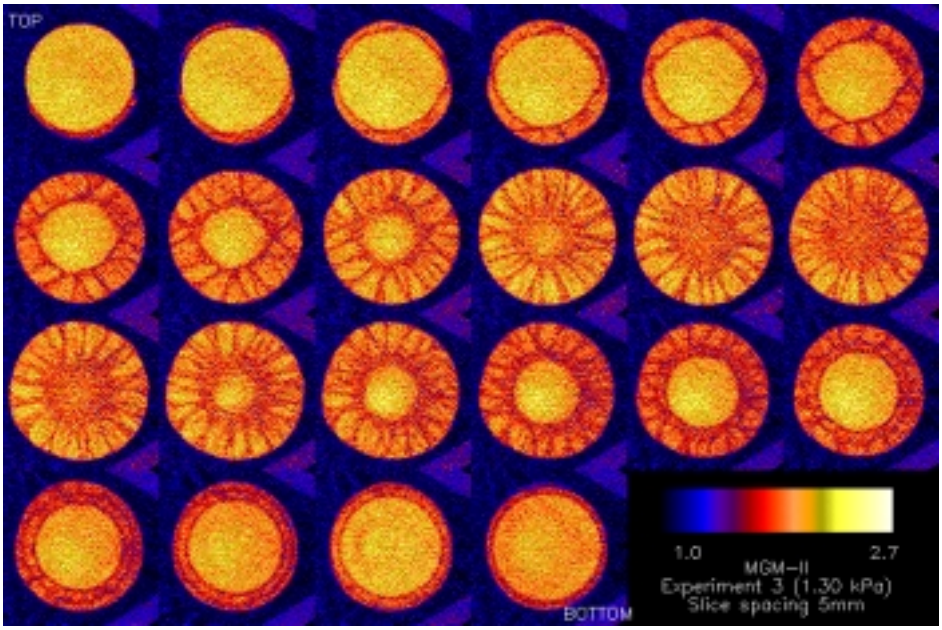

Figure 22. Example of horizontal slices through F2 specimen acquired by CT scanning.

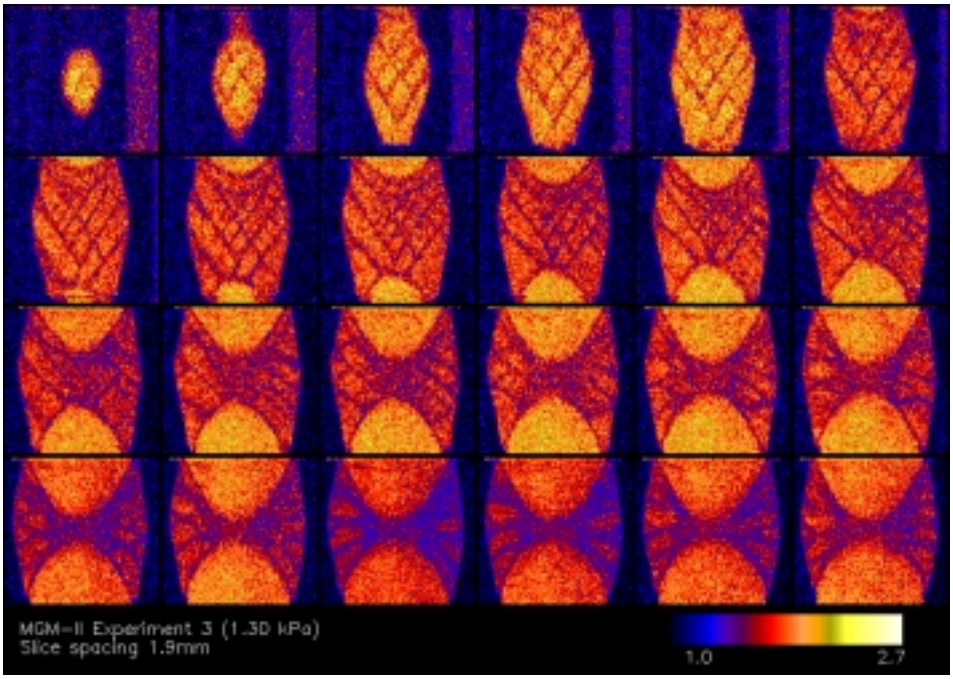

Figure 23. Example of vertical slices through F2 specimen acquired by CT scanning.

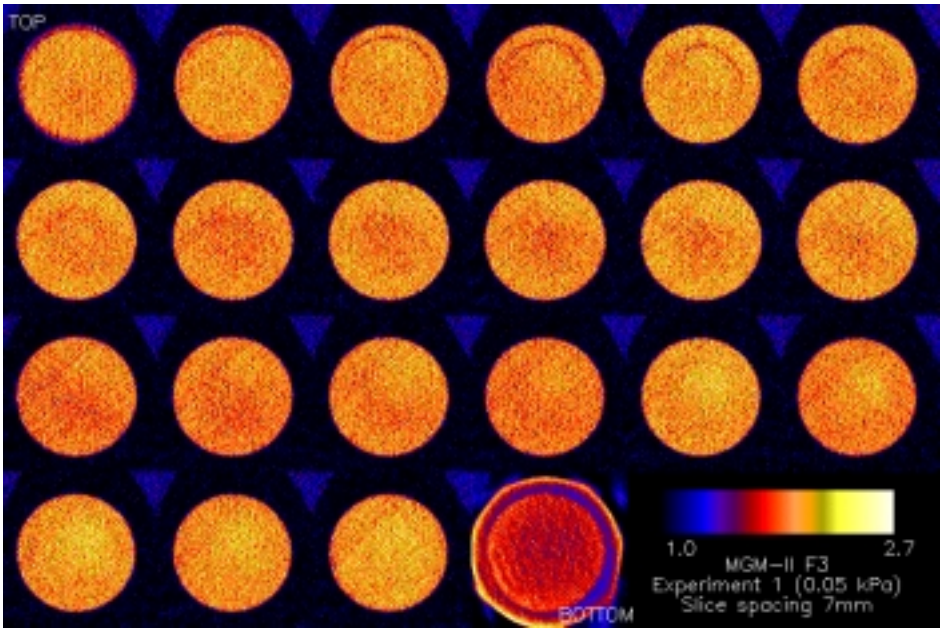

Figure 24. Example of horizontal slices through F3 specimen acquired by CT scanning.

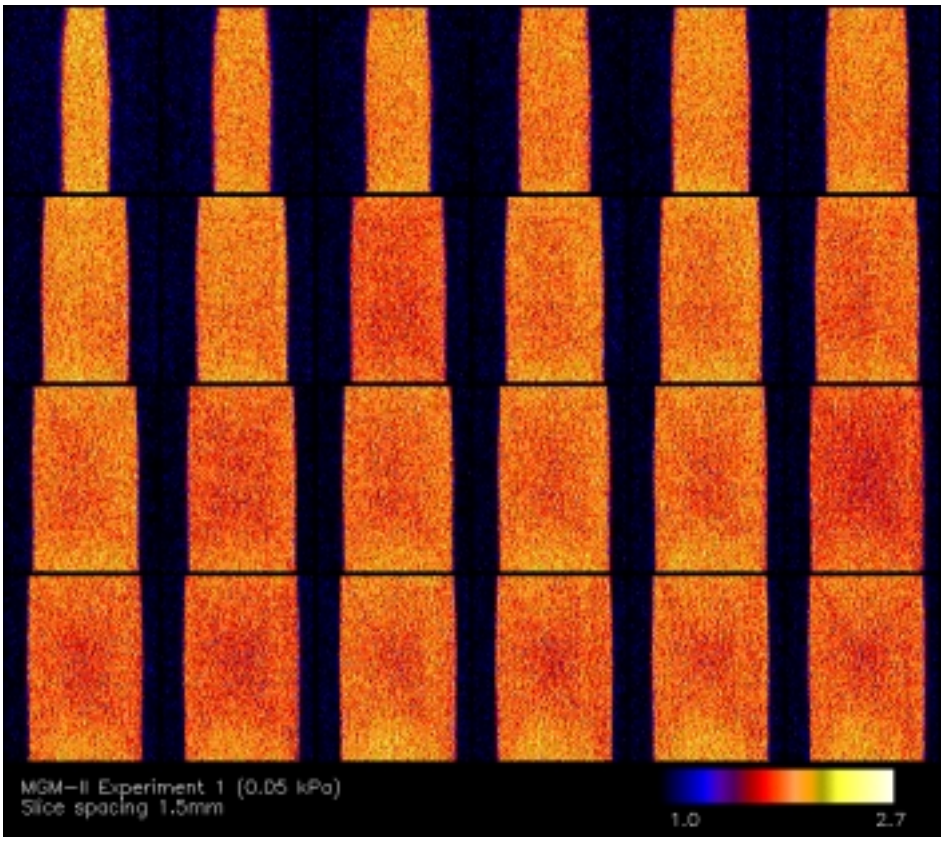

Figure 25. Example of vertical slices through F3 specimen acquired by CT scanning.

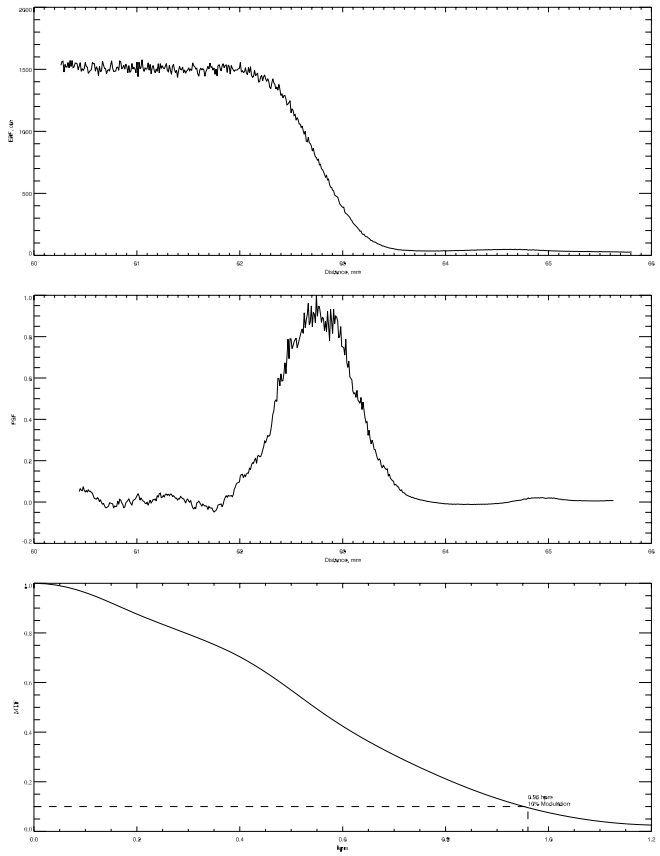

Figure 26. Point spread function and modulation transfer function of an aluminum specimen from LANL data.

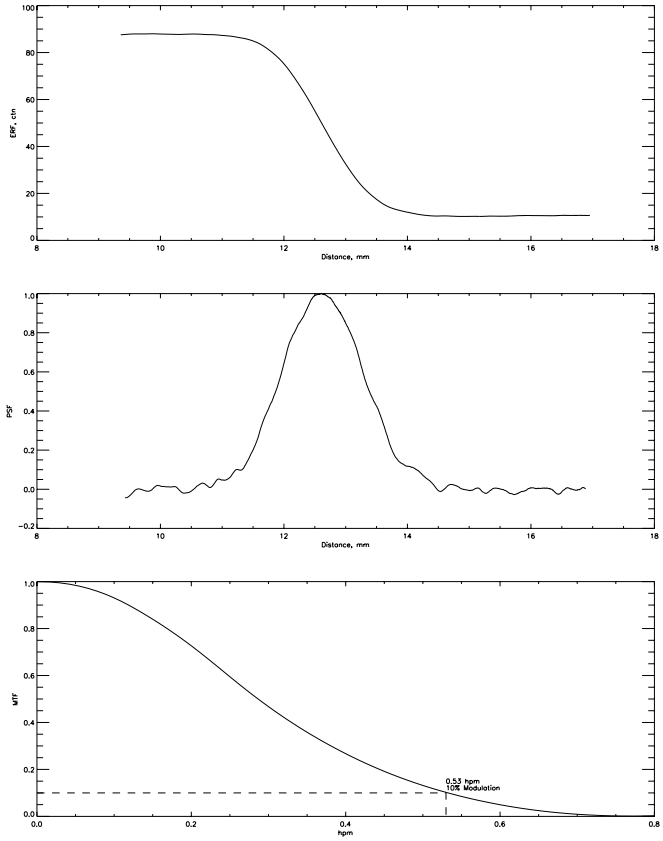

Figure 27. Point spread function and modulation transfer function of an aluminum specimen from KSC data.

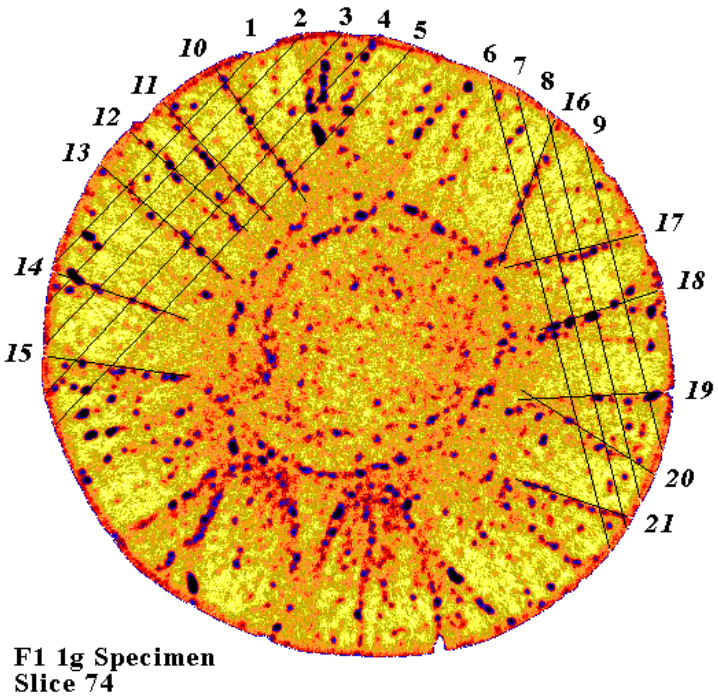

Figure 28. Image of cross-section of F1 1g specimen. Shear bands are numbered and profile lines indicated.

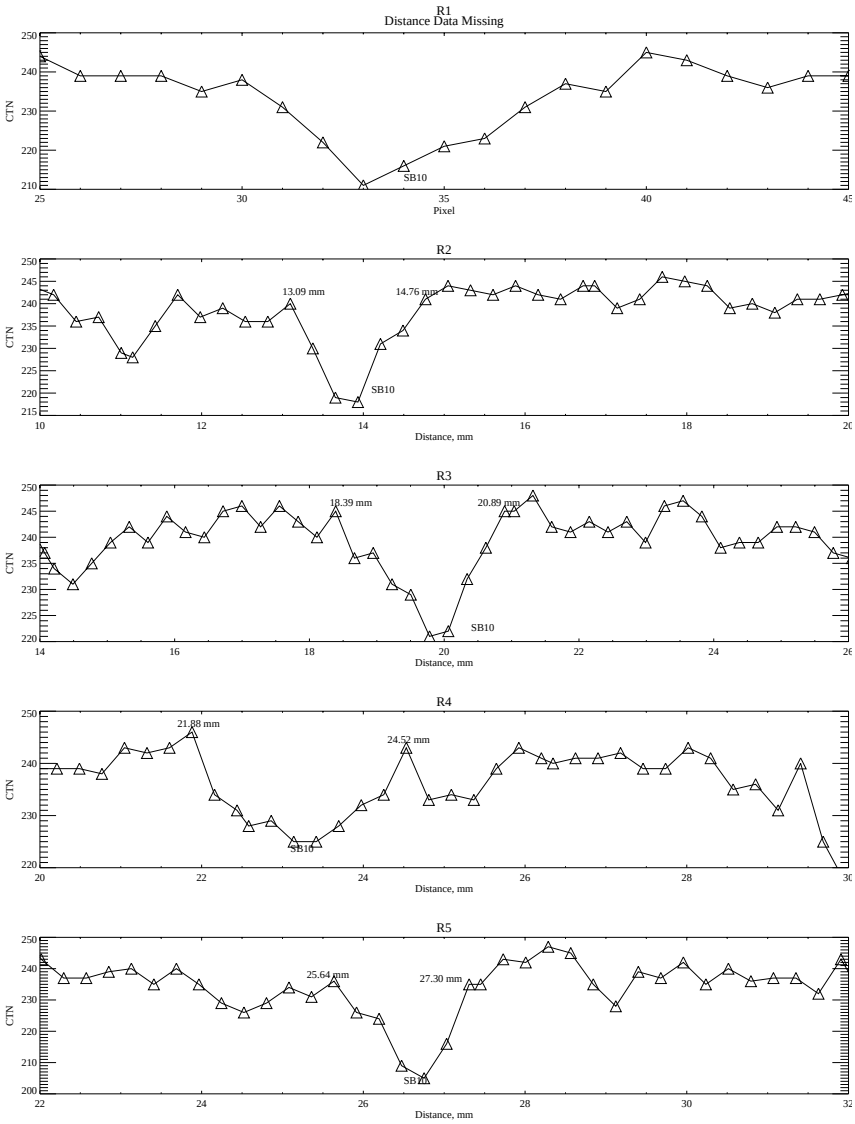

Figure 29. Quantitative data on shear band width and density from Figure 28.

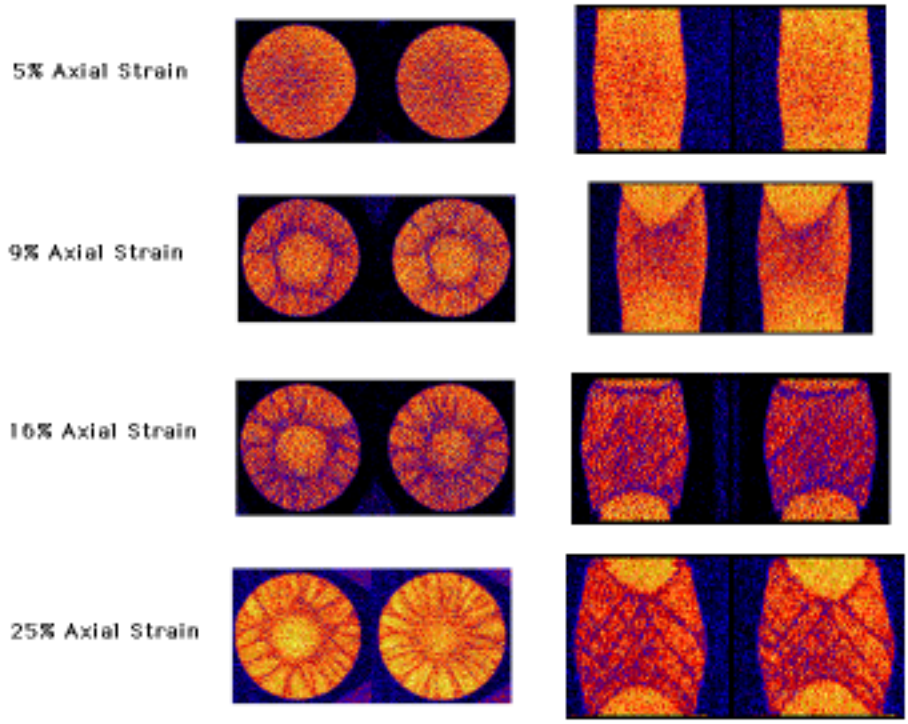

Figure 30. A progression of dense specimens tested at 1.30 kPa to various levels of compression indicate shear band formation.

6.3.4 SAMS

The SAMS data from the triaxial accelerometer sensors that recorded accelerations during MGM experiment operations on the STS/MIR missions are used for identifying and characterizing on-orbit events that may have had an impact on MGM experimental results. For the case of MGM-I flown on STS-79/MIR-04, the C-head SAMS sensor was mounted in near proximity to the TDLA on the forward pressure bulkhead of SPACEHAB and recorded accelerations in three orthogonal axes for each of three MGM experiments of that mission. For the STS-89/MIR-08 mission, the TDLA was mounted on the aft bulkhead with the A- and B-head SAMS acceleration sensors mounted nearby to monitor the microgravity environment during the six MGM experiments performed.

Sample SAMS data in Figure 31 shows acceleration values for the X, Y and Z axes during a portion of one MGM-I flight experiment. The acceleration environment on the X-axis was most active during the 12-minute period shown with 605 values outside the limits of ± 1 milli-g (mg) established in the MGM Science Requirements Document (SRD), while the Y- and Z-axes exhibited 24 and 287 values out of limits, respectively. The SAMS C-head sampling frequency was approximately 125 Hz; the frequency response was 0.01-25 Hz. The Y-axis data is typical of most periods during the experiments. The X-axis data reveals higher vibration activity, which occurred during several periods for each sensor axis during each experiment, but was generally short-lived.

For each of three MGM-I experiments, SAMS accelerometer data have been plotted and examined for g-value excursions that exceed the desired limits. For the overall duration of MGM Experiment-1, the largest deviations from 0-

g were -50.8mg and +51.4mg, and occurred near 02/01:16 MET during the deactivation phase of the experiment when no adverse effects likely occurred. The SAMS data show that a total of 12,426 g-measurements were outside the ± 1mg limits among 4.05M samples recorded during Experiment-1, representing 0.31% of the total data sample. For Experiment-2, the greatest deviations were -5.78mg and +8.79mg at about 03/23:51 MET. They occurred during the active phase of the experiment. There were 7354 out of limits samples out of 5.4M for the experiment duration, or 0.14%. Experiment-3 SAMS data showed largest deviations from 0-g of -9.79mg and +8.27mg near 04/21:18 MET, during active experiment operation. This experiment had 6800 out of bounds g-measurements representing 0.072% of a sample of 9.45M.

A comparison between SAMS data acquired during the three MGM-I flight experiments and load and pressure data recorded simultaneously has been completed. Two kinds of features were examined: accelerations larger than MGM requirements of ± 1 milli-g, and large, unexpected deviations in load and pressure data. By comparing the time of occurrence, and noting large acceleration levels immediately preceding load and pressure deviations, it may be determined if accelerations disturbed the experiments. Since load and pressure data are reasonable and continuous, it appears that as a whole the experiments were not adversely affected by accelerations. A few test data show, however, local areas of unexplained disturbance, such as small jumps or atypical values in pressure or load, though these small deviations do not appear to affect the overall long-term behavior of the specimens.

The SAMS data recorded during the MGM-II experiments have been acquired from the NASA Lewis Research Center (LeRC) server and have undergone detailed processing, plotting and comparison with MGM load and pressure data. The Principal Investigator Microgravity Services (PIMS) have provided plots of all SAMS data for the time periods of the experiments. These plots show only acceleration data within the ± 1 mg bandwidth, but indicate the times of larger deviations, and denote the minimum and maximum accelerations and respective times during the 30-minute intervals of the plots. Overall the acceleration levels were within requirements during the active phase of all six experiments and were similar to those of the MGM-I mission. There are discrete acceleration events during each of the MGM-II experiments recorded on each axis of both A and B sensor heads for which accelerations exceeded ± 1 milli-g, the smallest and largest in magnitude being –49.6 and +54.8 mg on the B-head Y axis near the end of the first F3 experiment as noted for the PIMS data in Figure 32. These deviations, like the ones of the previous flight, are short-lived, and upon thorough comparison with load and pressure data appear not to have adversely affected the MGM-II experimental results.

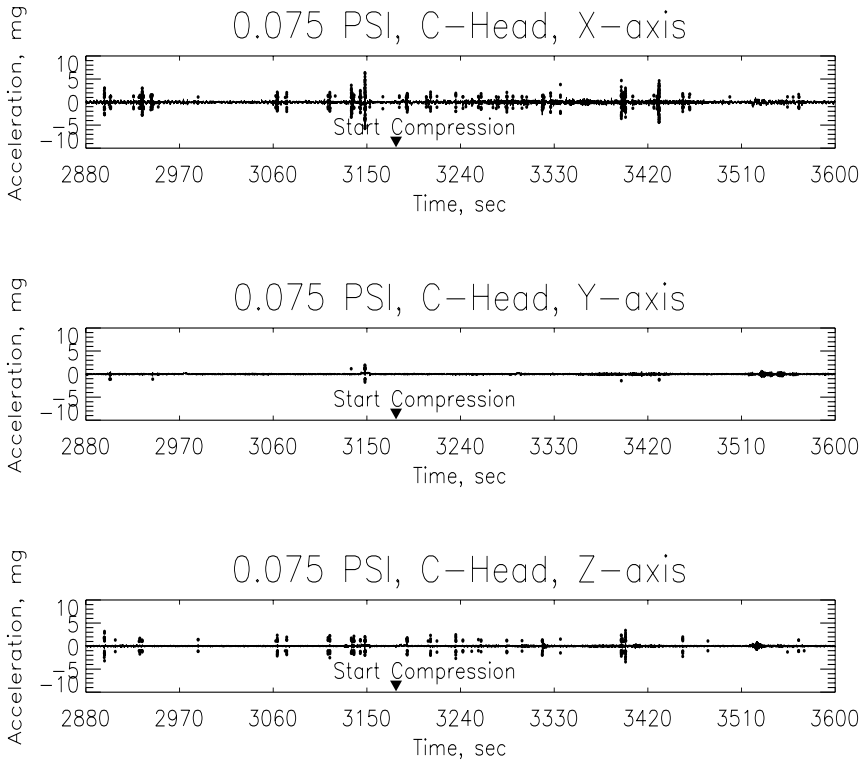

Figure 31. Example of SAMS data.

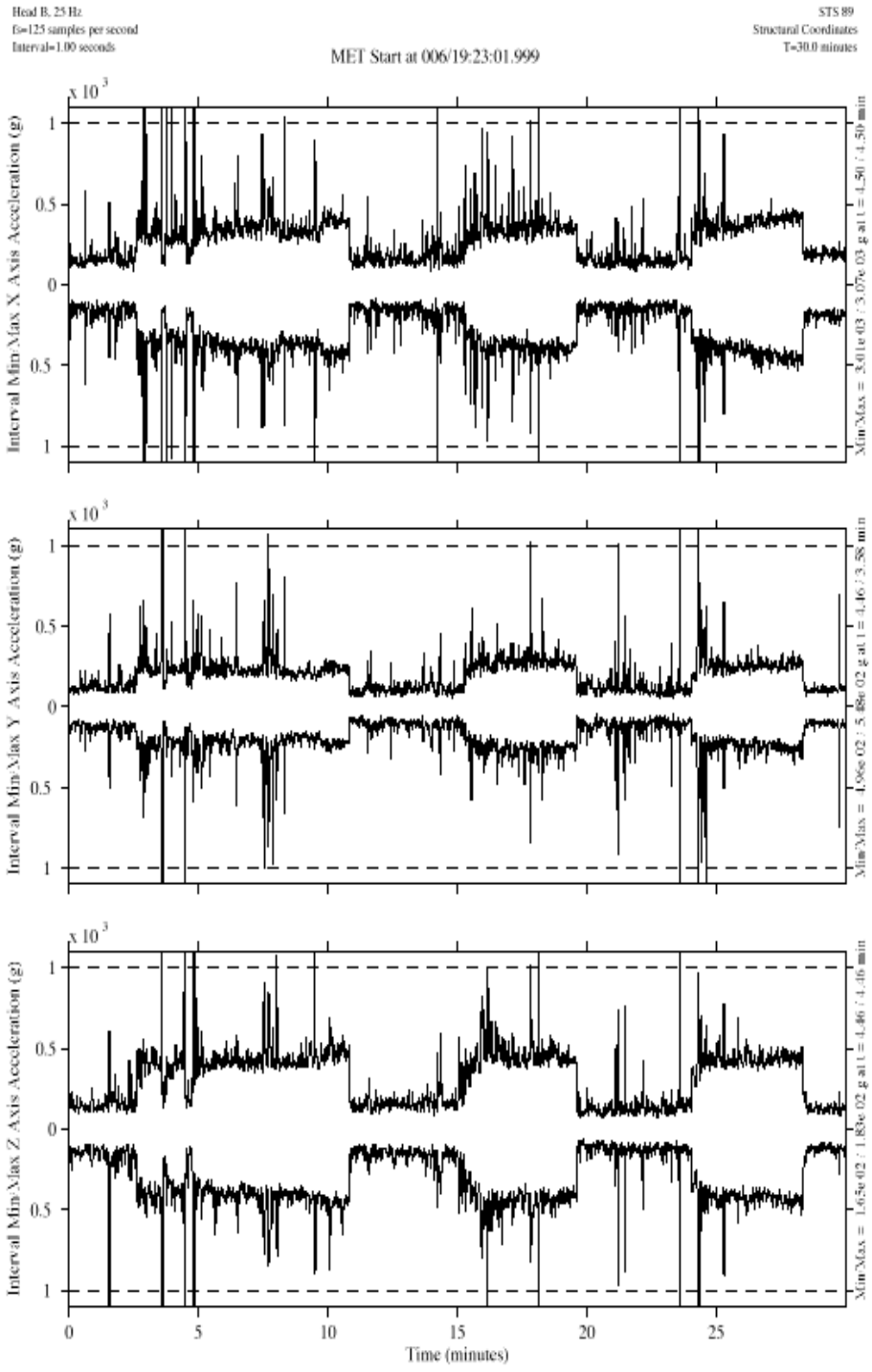

Figure 32. Example of SAMS data from PIMS.

6.4 Conclusions

The data processing and analysis effort thus far has been very successful and shows exciting results. Due to excellent equipment performance and data collection, there is complete science data return, which will aid greatly in completing a full analysis.

The microgravity tests indicate that the low confining pressures lend to high friction and dilatancy angles in cohesionless soil. Also, the overall volume change, in terms of expansion, and bifurcation instability, revealed in terms of relatively uniform bulging, are very new phenomena, which are currently being studied. Specimen shear and radial features are present in both MGM-I and MGM-II, and are being studied through CT information. While similarities are present and being studied between the two sets of data, differences are also important. In particular, the internal friction angles vary between MGM-I and MGM-II, as well as oscillatory behavior. The similarities and differences are being studied to understand how microgravity, low pressures, and density affect the behavior of a cohesionless material.

MGM-II has also revealed new data. The volumetric expansion during F2 experiments led to extremely low density specimens, lower than achieved during MGM-I. As a result, a new upper-bound relative density at critical state has been distinguished. Also, direct comparison of CT data between F2, F3 and terrestrial experiments has given researchers insight into the development pattern of shear band formations. The stability of the triaxial configuration leads to a late formation of shear bands, which in turn indicates the friction angle, dilatancy, and stiffness moduli measurements to properly represent constitutive behavior of the granular material at low effective confining stress.

Acknowledgments

The authors gratefully acknowledge support provided by NASA, Marshall Flight Center, Contract NAS8-38779 to the University of Colorado, Boulder. This material is also based in part upon work supported under a National Science Foundation Graduate Fellowship. We also wish to acknowledge advice and assistance at various stages of this project from Alfredo Baeza, Robert Habbit, George Alder, Todd Adelman, of Sandia National Laboratories, Martin Jones and David Stupin of Los Alamos National Laboratory, Peter Engel of the Kennedy Space Center Computed Tomography System, and Buddy Guynes, Tom Stinson, Jerry Shelby, John Oddo, Ron Cantrell, Ron Porter and Joel Kearns of NASA Marshall Space Flight Center.

7 Bibliography

Alshibli, K., N. Costes, and R. Porter. “Mechanics of Granular Materials.” Space Processing of Materials, International Symposium on Optical Science, Engineering, and Instrumentation, SPIE-The International Society for Optical Engineering, Denver, Colorado, Vol. 2809 (1996): 303-310.

Al-Shibli, K., E. Macari, , and S. Sture. “Digital Imaging Techniques for the Assessment of Homogeneity of Granular Materials.” *Emerging Technologies in Geotechnical Engineering, Transportation Research Record No. 1526, Transportation Research Board* (1996): 121-128.

Alshibli, K., et al. "Mechanics of Granular Materials Under very Low Effective Stresses in a Microgravity Environment", EOS Transactions, American Geophysical Union, Vol. 79, No. 17 (1998), pp. S333.

Alshibli, K., Sture, S., and Costes, N. C. "Effect of Inclusions on Plane Strain Behavior of Sand", 12th ASCE Engineering Mechanics Conference, La Jolla, California, 1998, pp. 1291-1294.

Alshibli, K. A., et al. "Assessment of Localized Deformations in Sand Using x-ray Computed Tomography", Accepted for Publication at ASTM Journal of Geotechnical Engineering, in press, 1999.

Alshibli, K. A. and Sture, S. "Sand Shear Band Thickness Measurements by Digital Imaging Techniques", Accepted for publication in "Imaging Technologies in Civil and Environmental Engineering", *Journal of Computing in Civil Engineering, ASCE*, Vol. 13, No. 2, pp. 103-109, (1999).

Alshibli, K. A., et al. “Constitutive Behavior of Sand Under Very Low Effective Stresses”, Presentation at the *NASA Third Phase 1 Research Program Results Symposium*, Nov 3-5, 1998, Huntsville, AL.

Alshibli, K. A., Sture, S., and Costes, N. C. “Constitutive and Stability Behavior of Soils in Microgravity Environment”, Accepted for publication in *Space Technology and Applications international forum (STAIF-2000): Conference on International Space Station Utilization*, to be held in Albuquerque, NM, Jan. 30 – Feb. 3, 2000.

Alshibli, K. A., Batiste, S. N., Swanson, R. A., Sture, S., Costes, N. C., and Lankton, M. “Quantifying Void Ratio Variation in Sand Using X-ray Computed Tomography”, Accepted for publication in *Geo-Denver 2000*, ASCE, Geo-Institute Congress to be held in Denver, CO, Aug 3-8, 2000.

Batiste, S. “Mechanics of Granular Materials at Low Confining Stress”: MS Thesis, University of Colorado at Boulder, 1998: 167 pages.

Bolton, M.D. “The Strength and Dilatancy of Sands.” Geotechnique, Volume 36, No. 1 (1986): 65-78.

Costes, N. C., and S. Sture. "The Potential of In-Space Research on Liquefaction Phenomena and Related Soil Behavior." International Conference on Recent Advances in Geotechnical Earthquake Engineering and Soil Dynamics," Proceedings Volume III, St. Louis, Missouri (1981): 929-959.

Costes, N. C., V. C. Janoo, and S. Sture. "Microgravity Experiments on Granular Materials." Materials Processing in the Reduced Gravity of Space, Symposium of the Materials Research Society, Volume 87 (1986): 203-211.

Costes, N. C. and S. Sture. "Mechanics of Granular Materials (MGM), Science Requirements." NASA/MSFC Document JA64-027, August 29, 1986.

Costes, N. C., V. C. Janoo, K. W. French, J. K. Parker, and S. Sture. "Mechanical Behavior of Cohesionless Granular Materials at very Low Inter-Granular Pressures." "Paper AIAA-87-0234." AIAA 25th Aerospace Sciences Meeting, Reno, Nevada, January 12-15, 1987.

Costes, N. C., S. Sture, and D. F. McTigue. "Mechanics of Granular Materials at Very Low Effective Stresses." ASCE Engineering Mechanics Conference, Texas A&M, College Station, Texas, May 24-27, 1992.

Costes, N. C., and S. Sture. "Issues on Geomechanics." Fifth International Symposium on Engineering, Construction, and Operations in Space, Albuquerque, New Mexico, June 1-6, 1996.

"E 1695-95: Standard Test Method for Measurement of Computed Tomographic (CT) System Performance", American Society for Testing and Materials. CD-ROM, Vendor. 1995.

Hettler, A., and I. Vardoulakis. "Behaviour of Dry Sand Tested in a Large Apparatus." Geotechnique, Volume 34, No. 2 (1984): 183-198.

Jaeger, H.M., and S.R. Nagel. "Physics of the Granular State." Journal of Science, Volume 255 (1996): 1523-1531.

Jaeger, H.M., S.R. Nagel, and R.P. Behringer. "The Physics of Granular Materials." Physics Today, April 1996: 32-38.

Jaeger, H.M., and S.R. Nagel. "Dynamics of Granular Material." American Scientist, Volume 85 (1997): 540-545.

Jeremic, B. "Finite Deformation Hyperelasto-Plasticity of Geomaterials." Ph.D. dissertation, University of Colorado at Boulder, 1997: 155 pages.

Lade, P.V., and M.J. Prabucki. "Softening and Preshearing Effects in Sand." Journal of Soils and Foundations, JGS, Volume 35, No. 4 (1995): 93-104.

Larsson, R., K. Runesson, and S. Sture. "Embedded Localization Band in Undrained Soil Based on Regularized Strong Discontinuity - Theory and FE Analysis." International Journal of Solids and Structures Volume 33, No. 20 (1996): 3081-3101.

Runesson, K., D. Peric, and S. Sture, "Effect of Pore Fluid Compressibility on Localization in Elastic-Plastic Porous Solids under Undrained Conditions," International Journal of Solids and Structures. Volume 33, No. 10 (1996): 1501-1518.

Scholz, C.H. Mechanics of Earthquakes and Faulting, Cambridge University Press, 1990.

Sture, S., K. Runesson, and E.J. Macari-Pasqualino. “Analysis and Calibration of a Three-Invariant Plasticity Model for Granular Materials.” Journal de Ingenieur-Archiv, Volume 59 (1988): 253-266.

Sture, S., et al. “Mechanics of Granular Materials Experiment.” NASA MSFC report, University of Colorado, 1995.

Sture, S., et al. “Mechanics of Granular Materials at Low Effective Stresses.” ASCE Journal of Aerospace Engineering. Volume 11, No. 3 (1998): 67-72.

Swanson, R., et al. "Mechanics of Granular Materials at Low Effective Stresses", Poster, EOS Transactions, American Geophysical Union, Vol. 79, No. 17 (1998), pp. S332.

Swanson, R., et al. "Behavior of Granular Materials in Microgravity at Very Low Effective Stresses", Poster Presentation at the 4th Microgravity Fluid Physics & Transport Phenomena Conference, Aug. 12-14,1998, Cleveland, OH.

8 Index of Tables and Figures

9 Acronyms

ARC	Ames Research Center
CEU	Combined Electronics Unit
CT	Computed Tomography
FO	Functional Objective
HW	Hardware
KSC	Kennedy Space Center
LANL	Los Alamos National Laboratory
LASP	Laboratory for Atmospheric and Space Physics
LeRC	Lewis Research Center
MGM	Mechanics of Granular Materials
MLE	Middeck Locker Equivalent
MSFC	Marshall Space Flight Center
NAS	National Academy of Science
NRC	National Research Council
PACE	Physics and Chemistry Experiments in Space
PGSC	Payload and General Support Computer
PI	Principal Investigator
PIMS	Principal Investigator Microgravity Services
PIP	Power Interface Panel
PSID	Pounds per Square Inch Differential
PSIG	Pounds per Square Inch Gauge
SAMS	Space Acceleration Measurement System
SNL	Sandia National Laboratories
SPPF	SPACEHAB Payload Processing Facility
SRD	Science Requirements Document
STS	Space Transportation System
TDLA	Twin Double Locker Assembly
UCB	University of Colorado at Boulder
VCR	Video Cassette Recorder
VIU	Video Interface Unit